Nasa CR-65222

GENERAL MOTORS CORPORATION

SUMMARY REPORT OF

EXPERIMENTAL INVESTIGATIONS OF SIMULATED METEOROID DAMAGE TO VARIOUS SPACECRAFT STRUCTURES

FACILITY FORM 602

N66-18182 (ACCESSION NUMBER) (THRU) 1

92 (PAGES) (CODE)

CR-65222 (NASA CR OR TMX OR AD NUMBER) 32 (CATEGORY)

Prepared For

National Aeronautics and Space Administration
Manned Spacecraft Center, Houston, Texas
Under Contract No. NAS 9-3081

GM DEFENSE RESEARCH LABORATORIES

SANTA BARBARA, CALIFORNIA

AEROSPACE OPERATIONS DEPARTMENT

GPO PRICE $ ______

CFSTI PRICE(S) $ ______

Hard copy (HC) 3.00

Microfiche (MF) .75

ff 653 July 65

TR65-48

JULY 1965

Copy No 11

GENERAL MOTORS CORPORATION

SUMMARY REPORT OF

EXPERIMENTAL INVESTIGATIONS OF SIMULATED METEOROID DAMAGE TO VARIOUS SPACECRAFT STRUCTURES

By C.J. Maiden , A.R. McMillan, R.E. Sennett, J.W. Gehring

Prepared For
National Aeronautics and Space Administration
Manned Spacecraft Center, Houston, Texas
Under Contract No. NAS 9-3081

GM DEFENSE RESEARCH LABORATORIES

SANTA BARBARA, CALIFORNIA

AEROSPACE OPERATIONS DEPARTMENT

TR65-48

JULY 1965

FOREWORD

This report represents a summary of the work performed under Contract NAS 9-3081 through 30 June 1965. A portion of the work described herein has been previously submitted in a draft paper titled "Spacecraft Hull Thickness Requirements for Protection Against Meteoroid Penetration", which was approved by NASA in May 1965 for presentation as a technical paper.

CONTENTS

ILLUSTRATIONS

INTRODUCTION

The results presented in this report represent an extension of the work in thin-shield impact published by two of the authors in an earlier AIAA paper.[1] Specifically, the structure that has been investigated consists of a thin shield (meteor bumper) spaced at a distance from the main hull of a spacecraft.

It is well established that the velocities of meteoroids relative to earth range from 11 to 72 km/sec; however, meteoroid density, flux, composition, etc. are not known with certainty.[2] Because of this general uncertainty in meteoroid properties, NASA has published an Engineering Criteria Bulletin[3] concerning the meteoroid environment to be used for spacecraft design. This environment is as follows:

(a) The isotropic flux-mass relationship for sporadic meteoroid is given by

$$\mathrm{Log}_{10} N = 1.34 \log_{10} m - 10.423 \quad (1)$$

where N is the number of impacts per square foot per day above mass, m, in grams.

(b) The density of meteoroids is 0.5 gm/cm^3 for all particle sizes.

(c) The average geocentric velocity is 30 km/sec for all particle sizes.

(d) The anisotropic flux during a shower is given by

$$\mathrm{Log}_{10} N = -1.34 \log_{10} m - 2.68 \log_{10} V - 6.465 + \log_{10} F \quad (2)$$

where V is the geocentric velocity of the meteoroid stream (km/sec), and F is the ratio of accumulative meteoroid stream flux to the sporadic meteoroid flux.

The isotropic flux relationship (Equation 1) can be used to calculate the critical meteoroid mass for various missions in space[2] (Figure 1). For example, the Apollo service module with a surface area, A, of 51 square meters, a 0.999

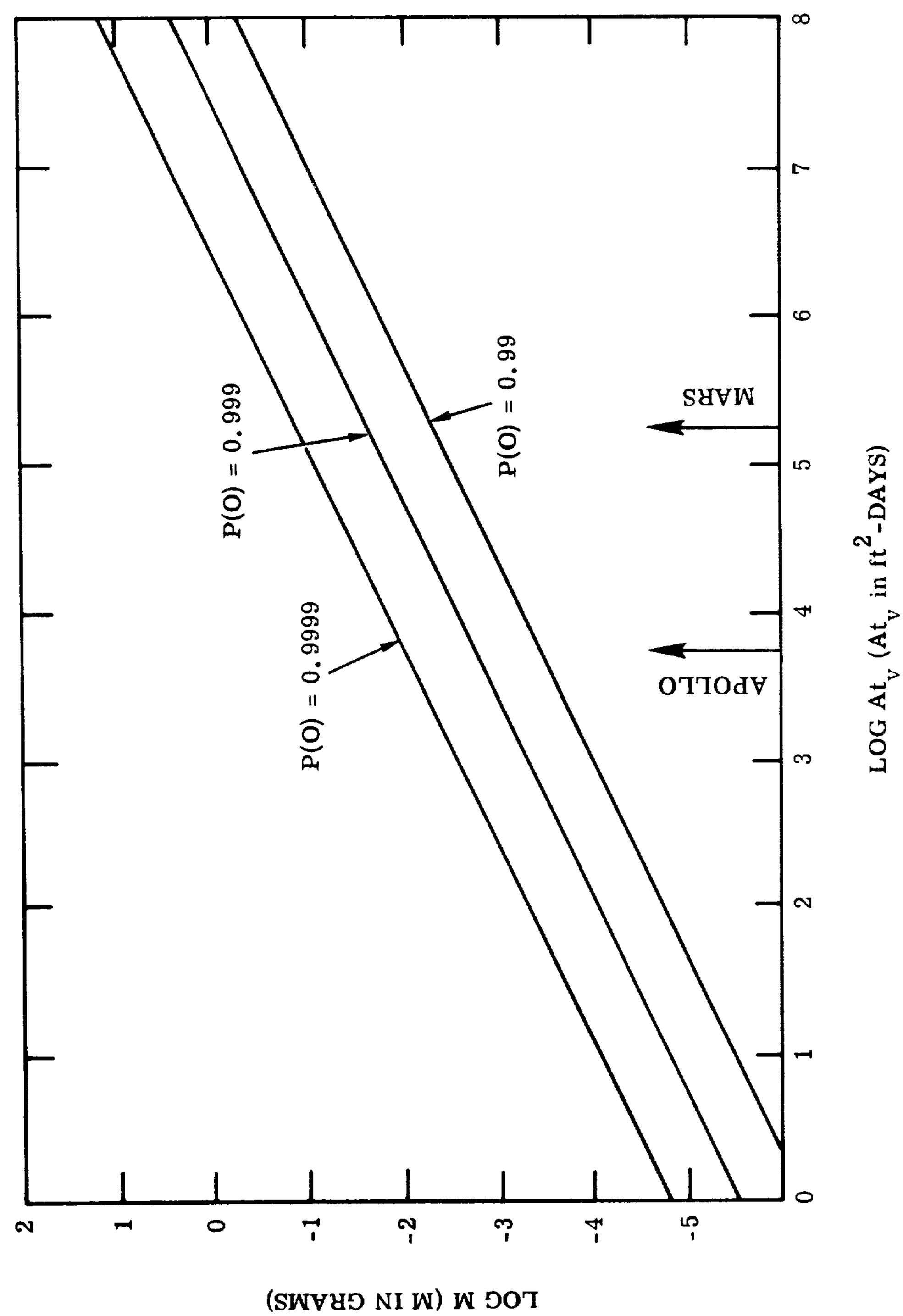

Figure 1 Mass of Largest Meteoroid Expected vs Mission Exposure

probability of no puncture, P(0) , and a mission time, t_y , of 14 days has to be protected against a meteoroid of mass 1.48 x 10^{-3} grams. This mass corresponds to a meteoroid with a diameter of 1.78 mm and a density of 0.5 gm/cm^3, or an aluminum particle with a diameter of 1.02 mm. Unfortunately, complete simulation of meteoroids in the laboratory has not yet been achieved.

Light-gas guns such as those used in the present study(4) are limited to velocities below 10 km/sec, and it is difficult to launch particles of meteoroid density even up to this velocity. For these reasons, the present study has been directed towards understanding the physics of impact in order to permit confident extrapolation of the results to extreme meteoroid velocities. In addition, the main emphasis has been placed on determining the optimum (minimum weight) structure for meteoroid protection.

3.2mm STEEL SPHERE
7 KM/SEC
1.016 mm NICKEL SHIELD

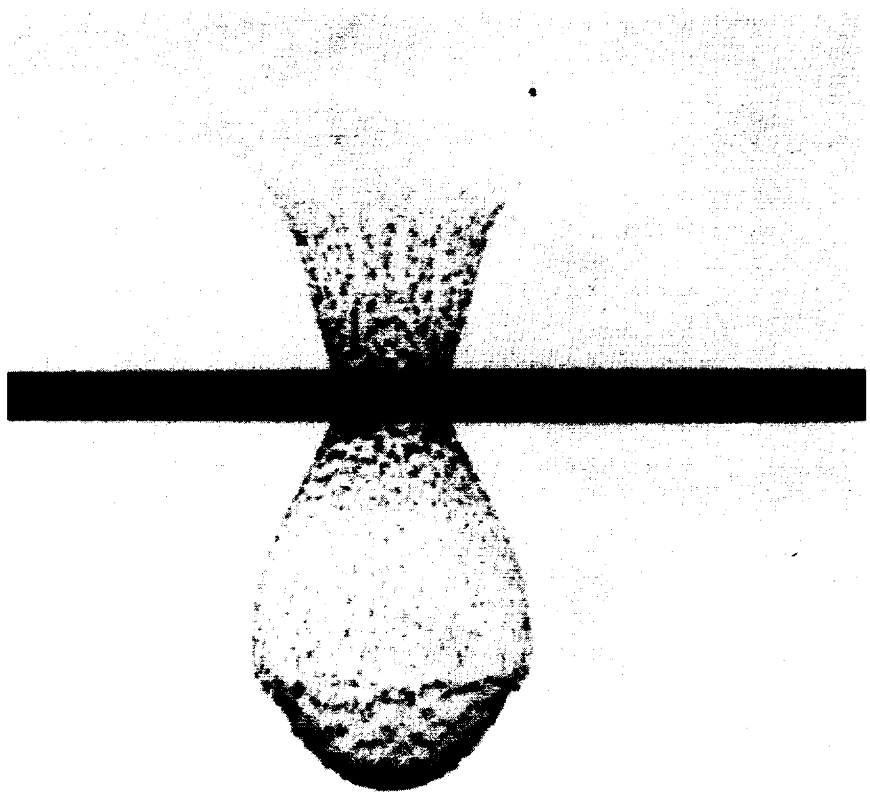

FIGURE 2 X Ray of Thin Sheet Impact

INTERACTION OF A HYPERVELOCITY PARTICLE WITH A THIN SHIELD

A flash X-ray of a particle-shield impact is shown in Figure 2. The physics of such an interaction was described in Reference 1 and the conclusions obtained can be summarized as follows:

(a) A shield is effective because it can fracture a hypervelocity particle, spreading its fragments and reducing their velocity below that of the original particle. If a shield is made too thin, its effectiveness at a given velocity is reduced because the spread of fragments is reduced, and fragment velocities tend to approach the velocity of the original particle.

(b) During the impact process, each element of the projectile and the shield is first shocked to some pressure and is then brought back to ambient pressure by release waves. This cycle is nonisentropic, and as a result the debris passing through the shield is heated. These heating effects are important in determining the size of fragments in the bubble. If the final debris is in the solid state, the size of fragments will decrease with increasing temperature because of a decrease in fracture strength. If the material is molten, only surface tension forces need to be overcome to create droplets; these forces, and hence the droplet size, will become smaller as the liquid becomes hotter. Finally, if the heating effects are great enough, the debris becomes vapor.

(c) An optimum shield is thick enough that the axial element of the shock (produced by the impact) reaching the back of a projectile is of sufficient strength to cause eventual melting of this element. Calculated optimum shield thicknesses as a function of impact velocity for aluminum projectiles and shields are shown in Figure 3. Note that the theory only applies at impact velocities above those necessary to cause melting. Also note that the optimum shield thickness decreases with increasing impact velocity.

(d) To a first approximation, shields of different materials but of equal weight are equally effective.

(e) The effectiveness of a shield is independent of the strength of the shield material at impact velocities above about 4 km/sec.

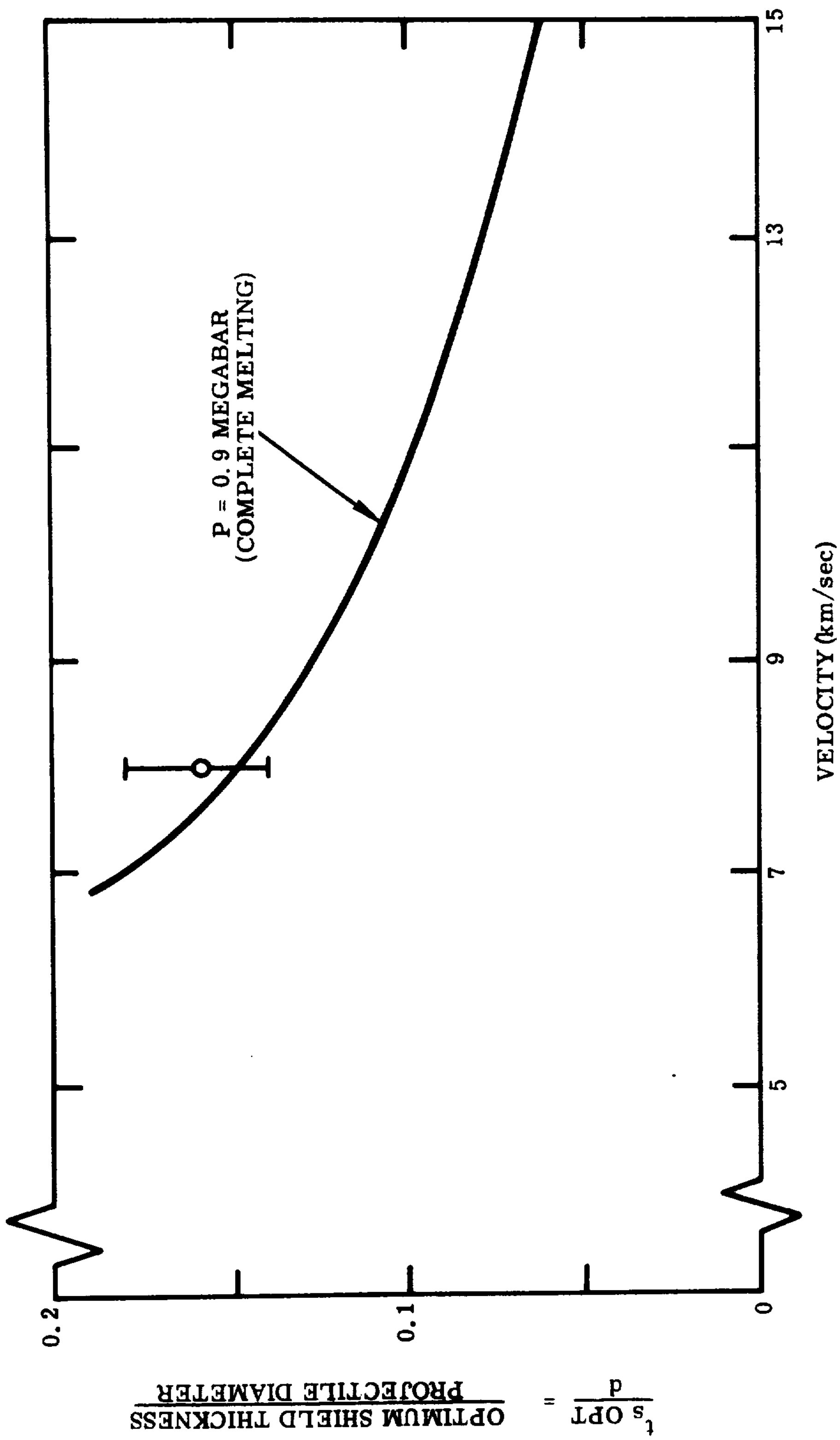

Figure 3 Optimum Shield Thickness-Aluminum Shield and Projectile

INTERACTION OF DEBRIS WITH A SHIELDED TARGET

THEORY

Preliminary Experiments

A series of experiments were made to investigate the types of failure that can result from the collective impact of debris on a shielded structure. In these experiments the projectiles were 3.2-mm aluminum spheres at 8.07 km/sec, the shields were 1100-0 aluminum 0.53-mm thick (near optimum, from Figure 3), the spacing was 5.08 cm, and the backup sheets were 7075-T6 aluminum with thicknesses 12.5, 9.6, 6.4, 3.2, 1.6 and 0.8 mm. Results of the tests (Figure 4) for the three thinnest sheets show that the 3.2-mm backup sheet was not penetrated, although a spall was almost detached; the 1.6-mm sheet has a spall partially detached and exhibits several tensile fractures; and the 0.8-mm target was completely perforated and shows the partial formation of several petals. A Beckman-Whitley framing-camera sequence of this last impact (Figure 5) reveals several interesting features. First, most of the damaging impulse does not occur across the full diameter of the bubble but over a central area with a diameter equal to about half the spacing, S . Second, this central area seems to be fairly uniformly loaded, for a definite step deflection can be seen in the early frames. Third, although a small spall detaches from the target, the main failure mode is tensile failure around the circumference of the loaded area. (Note that failure is not due to shearing as may first be supposed.)

The results above indicate that two failure mechanisms must be considered:

(a) Failure in tension due to the blast-loading effect of the debris impacting the target. Petalling is an example of such a failure.

(b) Failure due to the formation of a spall.

Initial theoretical attention has been given to the first mode of failure.

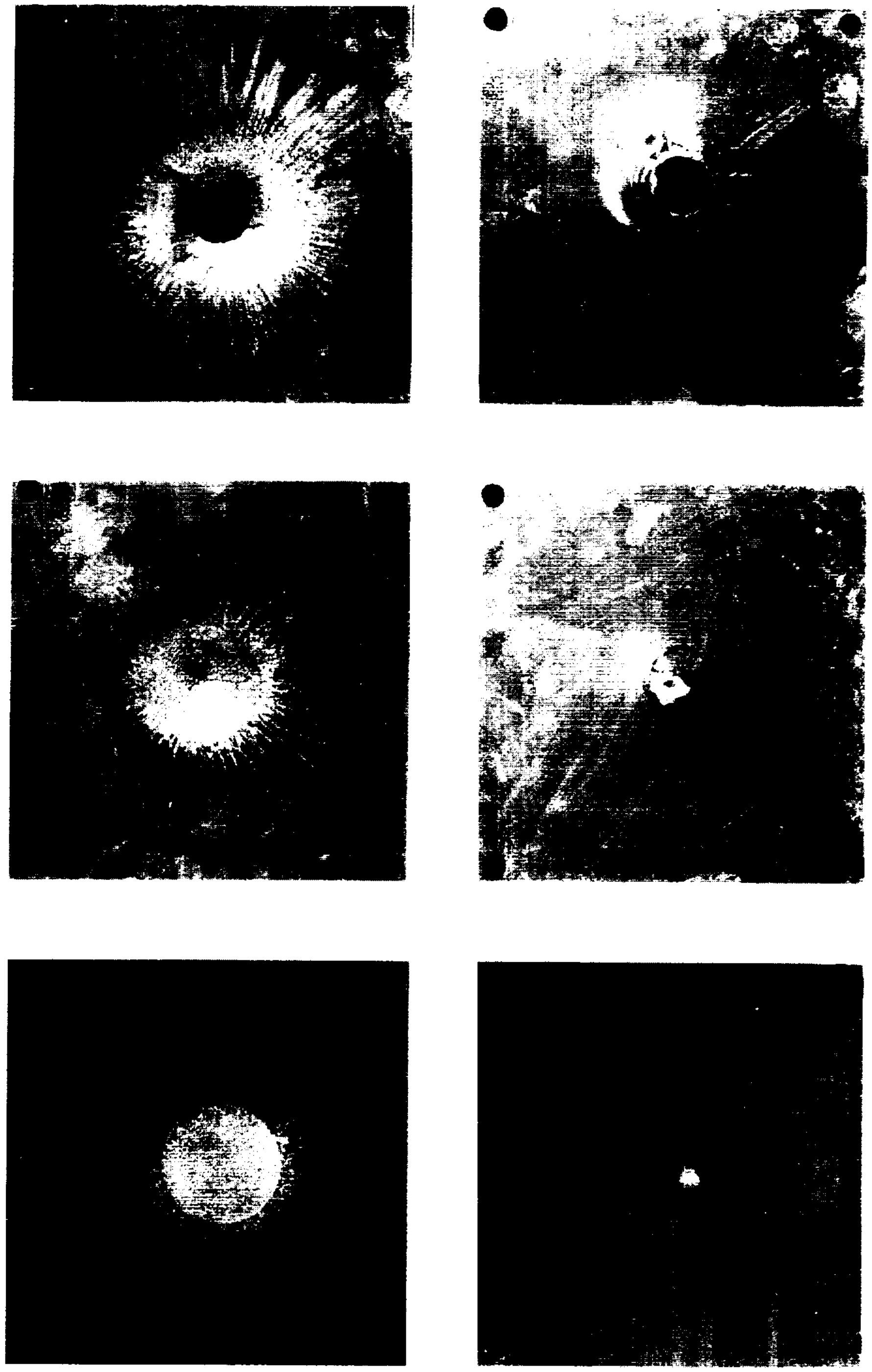

FIGURE 4 Effect of Backup Thickness

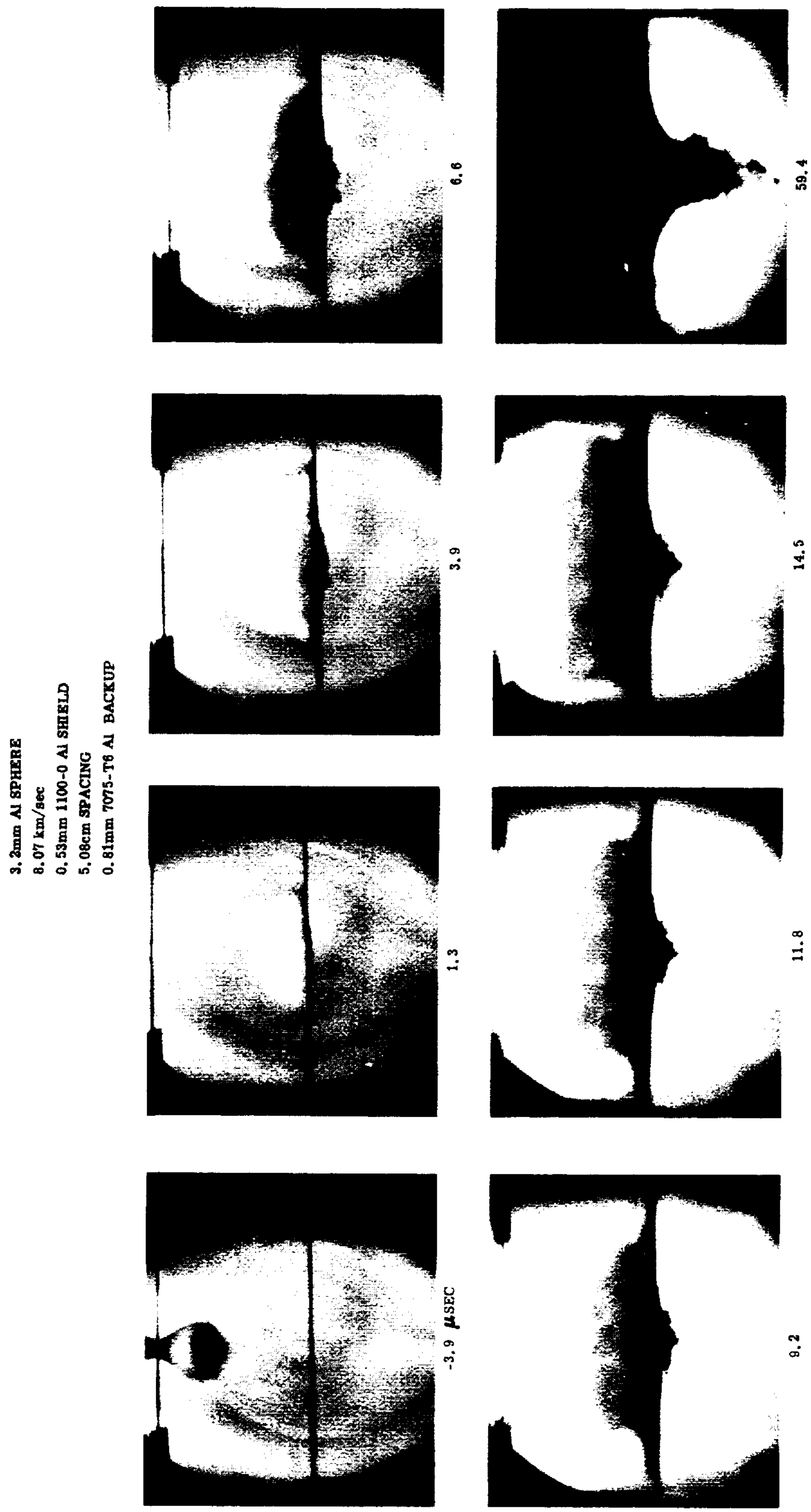

FIGURE 5 Framing Camera Sequence of Backup Failure

Theory of Failure of a Target Due to Gross Deformation

To treat this problem theoretically, such factors as the magnitude, distribution, and duration of the load applied to the target must first be determined. Then the large deformation dynamic response of the target has to be calculated, taking into account the elastic and plastic behavior of the target.

Assumed Loading

The following assumptions havebeen made:

(a) The load is uniformly distributed over a circular area of diameter equal to one-half the spacing.

(b) The load is applied so quickly that the loaded area is effectively given an initial velocity increment.

(c) The momentum transferred to the loaded area is equal to twice the momentum of the original particle.

Main justifications for assumptions (a) and (b) come from Figure 5, whereas a momentum multiplication factor of two, assumption (c), has been chosen for the following reasons: Since the impulsive load applied to a target increases with increasing impact velocity, a spacecraft inner hull must be designed to resist a meteoroid at the maximum expected velocity of 30 km/sec. At this velocity, the majority of the debris coming through the shield will be in gaseous form. Hence, if it is assumed that the momentum of the debris is equal to the momentum of the original particle and perfectly elastic collisions occur between each gas atom and the target, then the momentum multiplication factor should be two.

Large Dynamic Deformation Analysis

Given the loading, the next part of the problem is to determine the response of the target (assumed to be a thin shell). However, the problem of determining dynamic deformations and stresses in thin shells involves, in general, a complex system of nonlinear differential equations. For these problems that involve both large deflections and plasticity effects, a numerical technique has been developed by Witmer, et al.[5] This technique is based on a finite difference approximation for the original differential equations. These finite difference equations are then used to describe an equivalent lumped parameter model. For the time-wise step-by-step numerical analysis, the increments in stress resultants and stress couples are determined by idealizing the shell thickness as consisting of n concentrated layers (six layers were used in all the present calculations). Also, the material behavior used to determine the above increments can include elastic-perfectly plastic, elastic-strain hardening, or elastic-strain-hardening strain-rate-sensitive behavior.

The success of the above technique has been shown in a comparison of theory and experiment for explosively loaded beams in Witmer's paper.[5]

The Strip Approximation

Figure 6 shows the situation that was first investigated to determine the motion and stresses in the backup sheet.[6] In this approximation a strip (or beam) of material through the center of the loaded area has been considered. The rear sheet material has been taken as 7075-T6 aluminum. This material has been assumed to behave in an elastic-perfectly plastic manner with a yield strength σ_0 of 4.67×10^9 dynes/cm^2 (70,000 lb/in.^{2}) and a percentage elongation to fracture of 11 percent. The first step is to calculate the initial velocity v_i imparted to the central portion of the strip. From the previous assumptions, this is given by

$$v_i = \frac{32 M_p V_p}{\pi S^2 \rho_b t_b} \tag{3}$$

where M_p and V_p are the mass and velocity of the impacting particle; S is the spacing, and ρ_b and t_b are the density and thickness of the backup target. For the initial calculation, the following parameters were used: M_p = mass of 3.2-mm aluminum sphere, V_p = 7.63 km/sec, S = 5.08 cm, and t_b = 0.8 mm. Thus, this case corresponds to one of the preliminary experimental results shown in Figure 4.

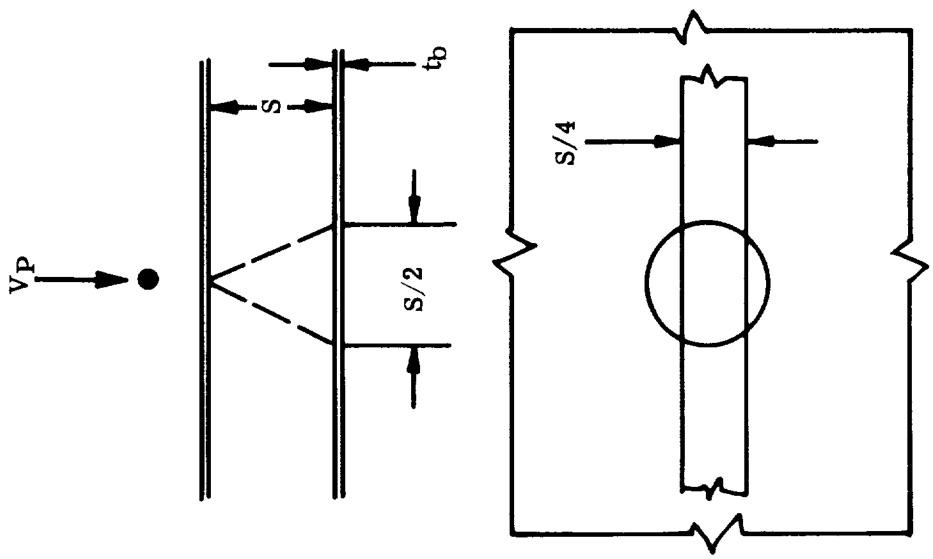

Figure 6 Strip Approximation

The results of the calculation are shown in Figures 7(a) and 7(b). The centerline deflection, the tensile strain at the edge of the loaded area, and the tensile strain at the center of the load are shown in these figures. Figure 7(a) includes the experimental curve of centerline deflection determined from the B&W photos (Figure 5), indicating good agreement between theory and experiment. Note that in Figure 7(b) the fracture strain is first reached at the edge of the loaded area after about seven microseconds; after this time the solution is academic. There is also some evidence of spalling in Figure 5, and such initial wave effects have been ignored for the moment.

The above calculations were repeated for a backup sheet 1.6-mm thick. The results showed that the peak strain occurs at the center of the sheet, and that the sheet should not fracture. Figure 4 shows that in practice only a small perforation occurs, and this is due to spallation.

The Effect of Span

With the above reasonable agreement between theory and experiment, it was decided to use the strip approximation further. Because solutions are required for an effectively infinite rear sheet, it was considered necessary to find out how long a strip is effectively infinite for the time of interest in the present problem. To do this, the first analysis (25.4-cm span) was repeated for a 50.8-cm span, with the result that up to about 100 microseconds no difference was found in centerline deflection, edge, or center strain for the two cases. Since in most situations of interest either the maximum or fracture strain would occur in less than 100 microseconds, it was decided that a 50.8-cm span would correspond to an effectively infinite sheet and would be used in all subsequent calculations.

Complete Results for Particles with a Diameter of 3.2 mm

The strip approximation was used to determine the response of backup sheets of various thicknesses for impacts of 3.2-mm particles at velocities of 7.62, 15.2, 22.8, and 30.4 km/sec. The results at 7.62 km/sec (Figures 8(a)–8(c)) show that there is a large difference between backup sheet thicknesses required for no-yield failure (maximum strain less than 0.7%) and no-fracture (maximum strain

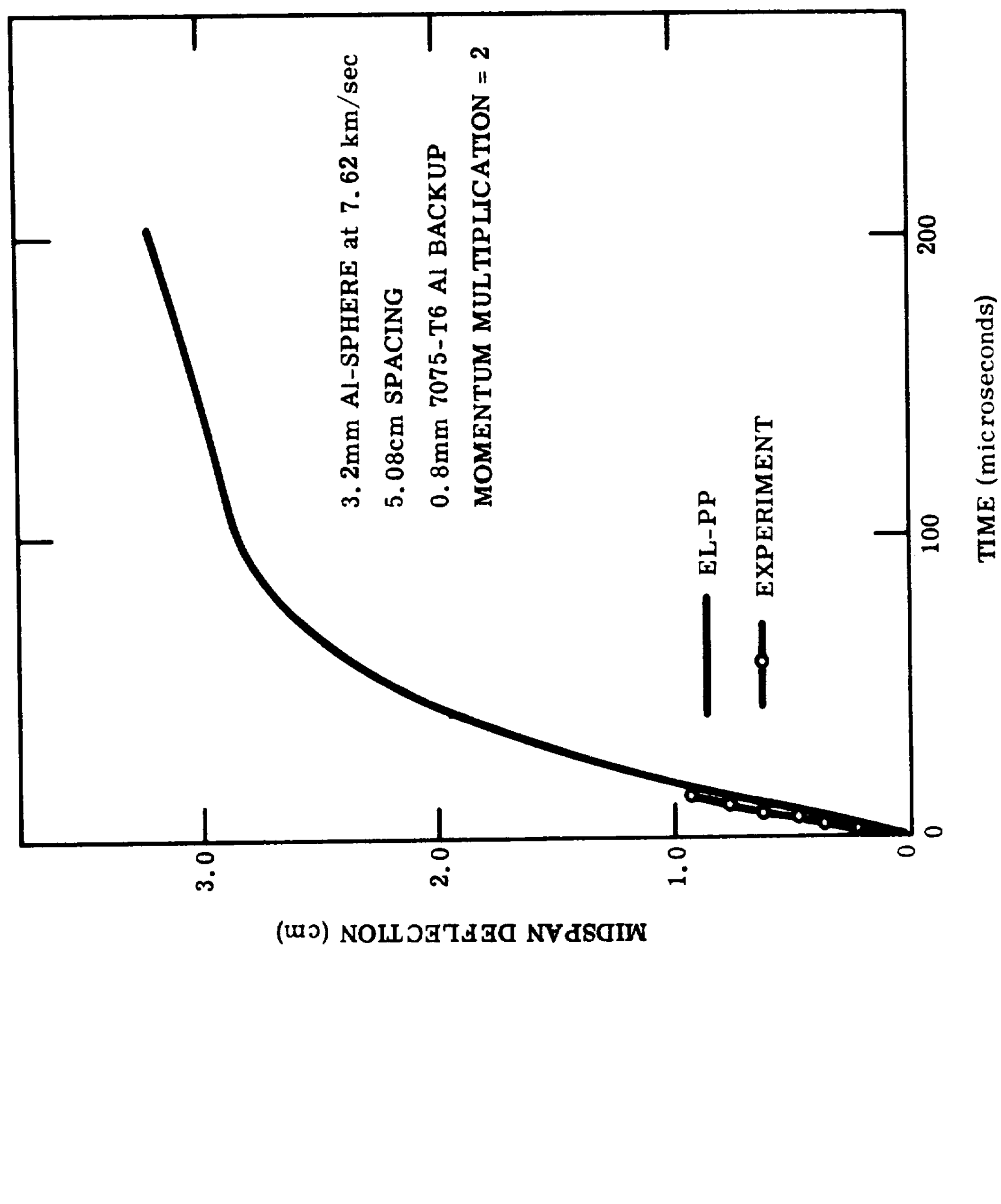

Figure 7(a) Time-Resolved Backup Sheet Calculations: Centerline Displacement vs Time

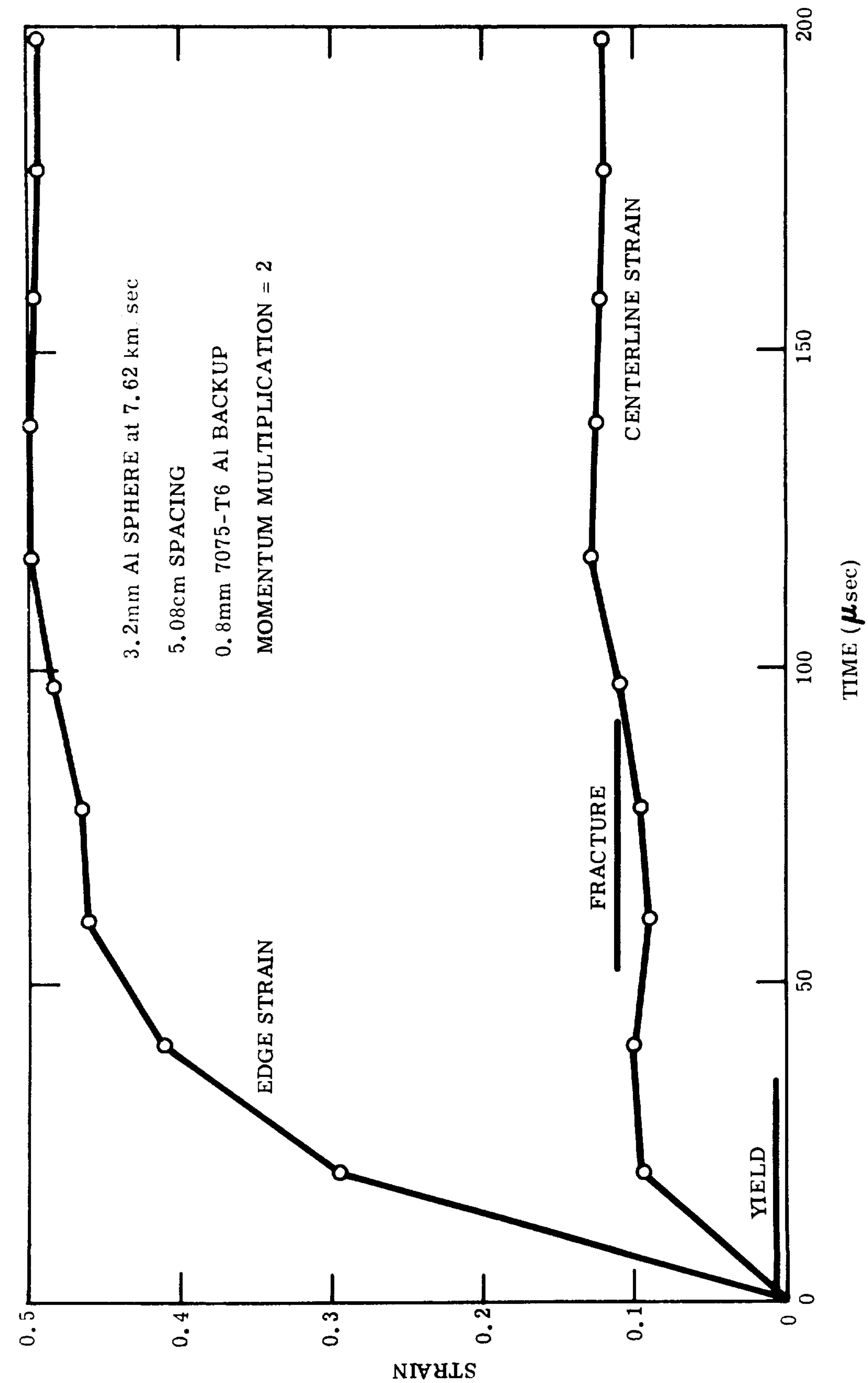

Figure 7(b) Time-Resolved Backup Sheet Calculations: Centerline and Edge Strain vs Time

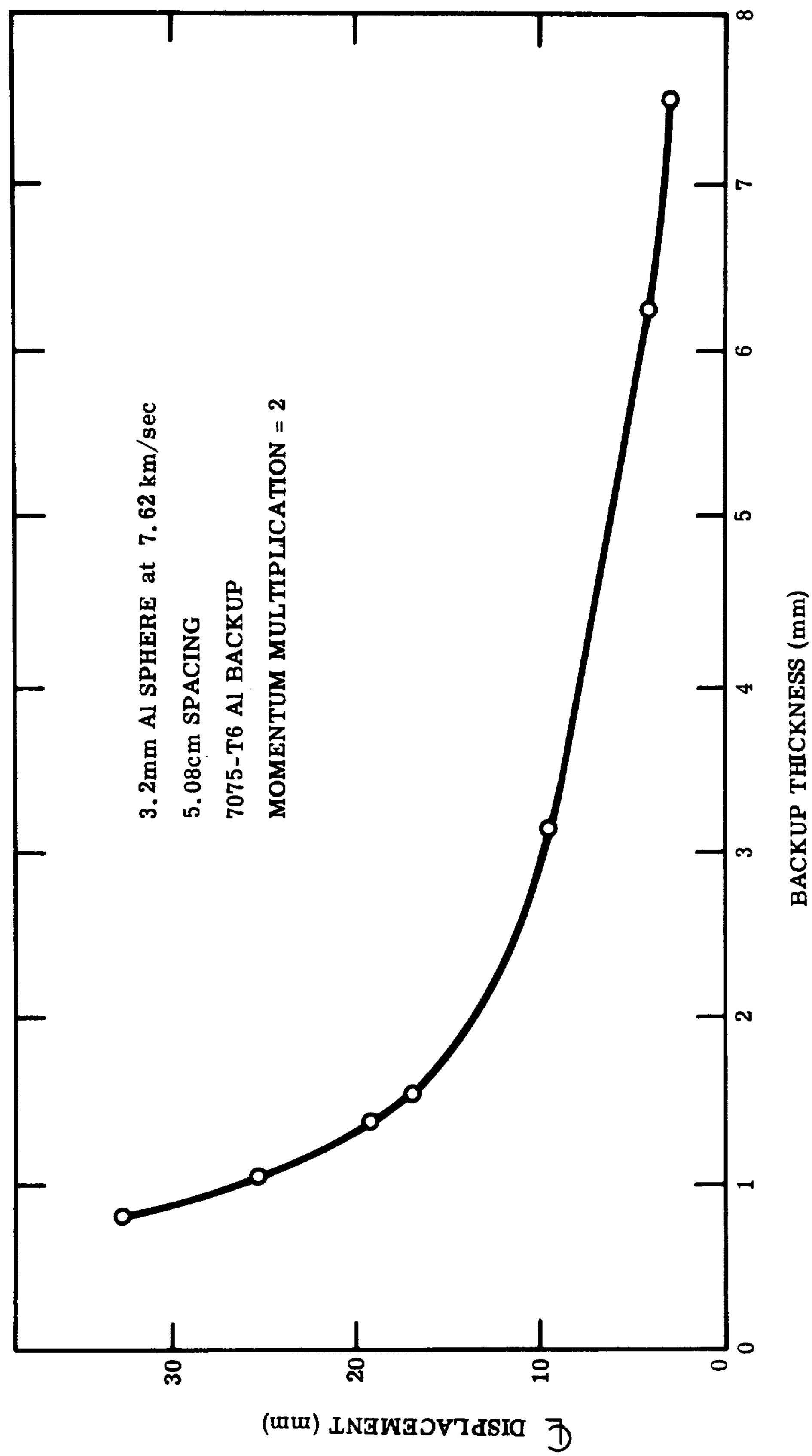

Figure 8(a) Effect of Backup Thickness on Backup Behavior: Centerline Displacement vs Backup Thickness at 200 Microseconds

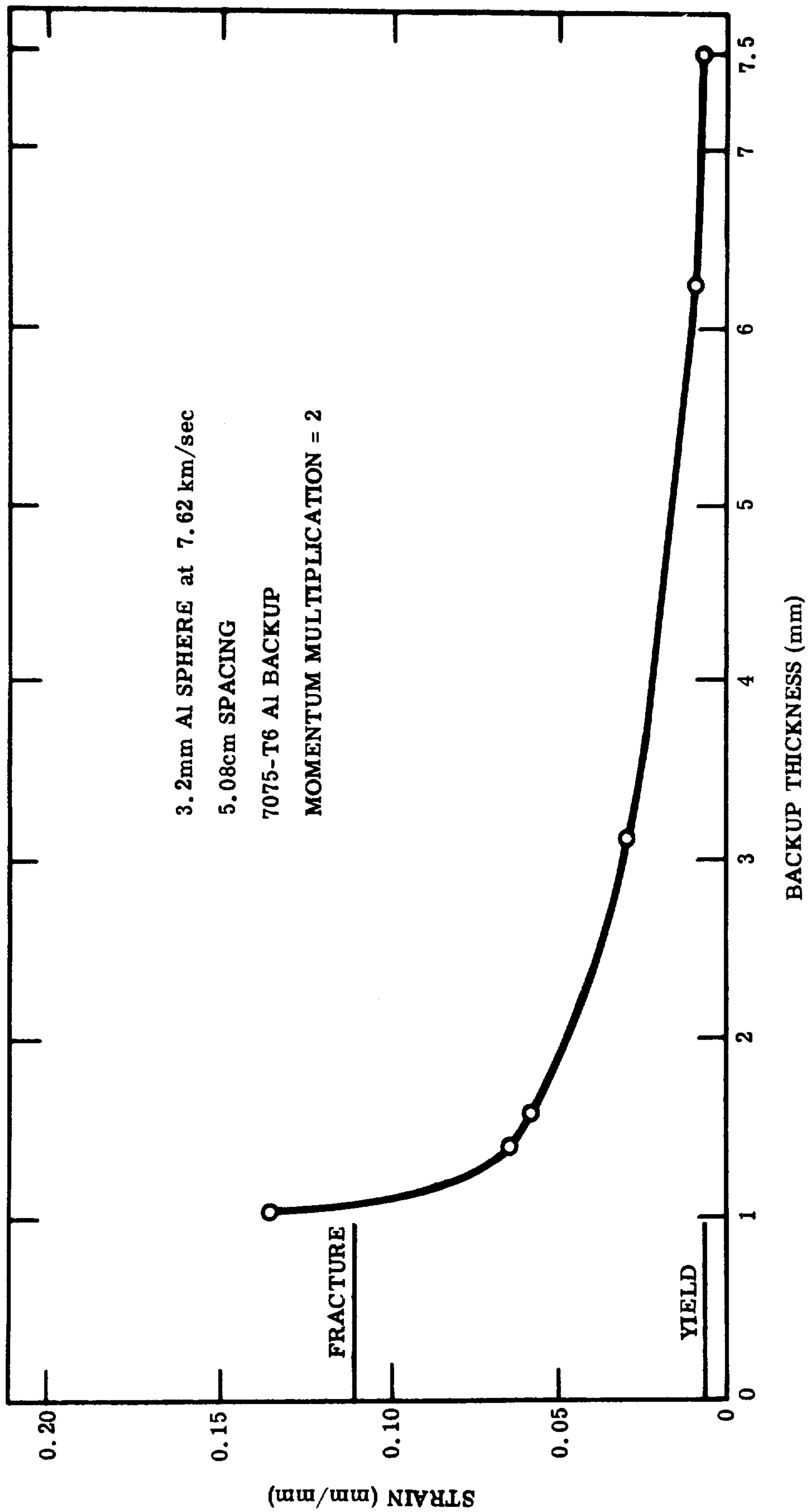

Figure 8(b) Effect of Backup Thickness on Backup Behavior: Maximum Centerline Strain vs Backup Thickness

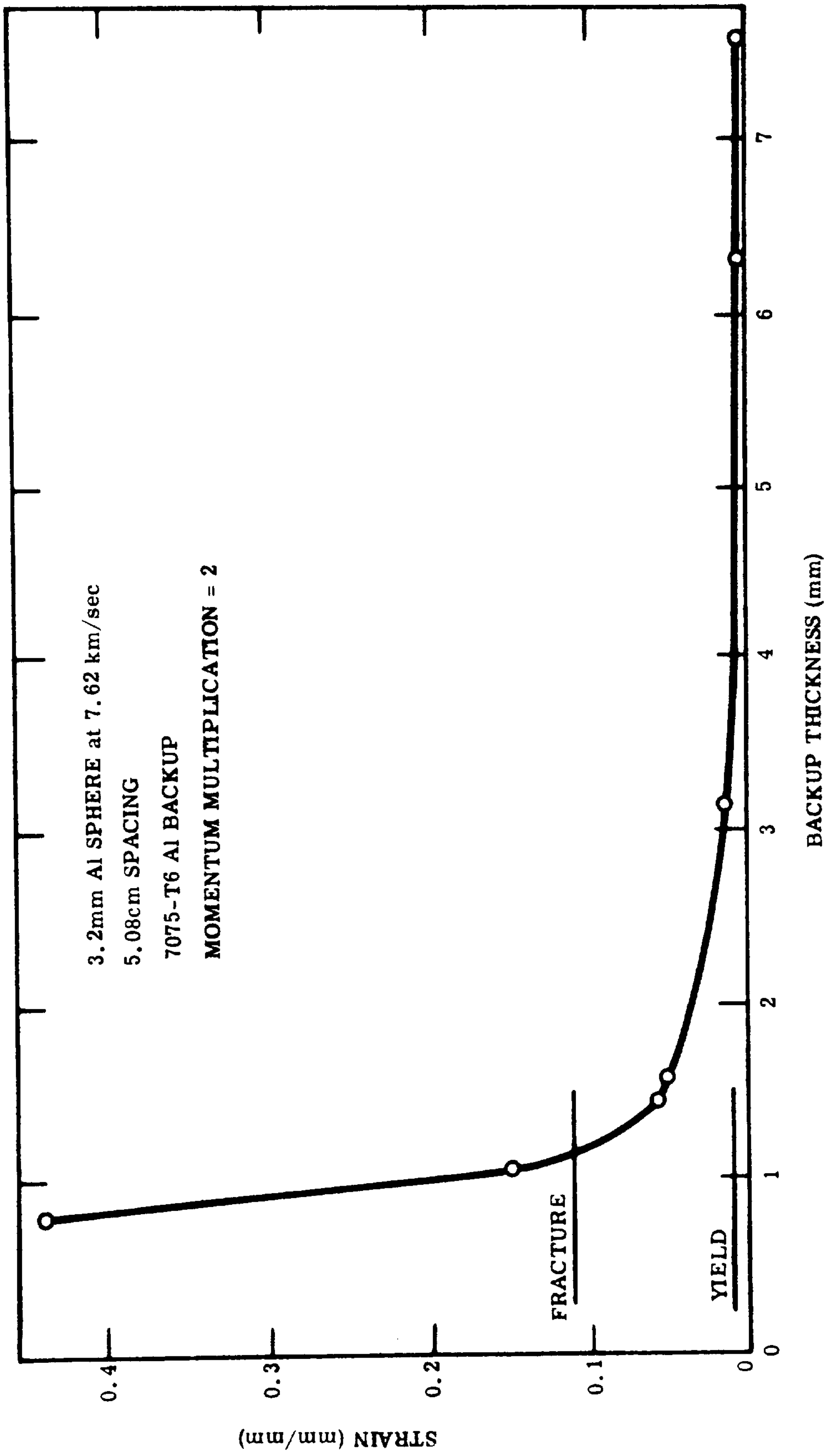

Figure 8(c) Effect of Backup Thickness on Backup Behavior: Maximum Edge Strain vs Backup Thickness less than 11%) failure. Also, it can be observed that for sheet thicknesses above about 1.6 mm the maximum strain occurs at the edge of the loaded area. Similar solutions to Figure 8 have been obtained for the other three impact velocities. The resulting curves of sheet thickness against impact velocity for failure criteria of yield, maximum strain of 2%, 4%, and 6%, and fracture are presented in Figure 9(a). The surprising aspect of this figure is that for each failure criterion the curve t_b against velocity is nearly linear. This is surprising in view of the fact that the basic mechanisms are nonlinear. It is also seen from this figure that, above about 4% maximum strain at a given velocity, a small decrease in thickness produces a large strain increment. Thus, it would appear wise to design for no more than a few percent maximum strain.

The Effect of Particle Size

Figure 9(b) shows results similar to those of Figure 9(a) but for 1.02-mm diameter aluminum spheres. The same comments can be made concerning the results for this particle that were made for the 3.2-mm particle. Note that the crowding of the constant maximum strain lines is seen to increase with decreasing particle size.

From the above figures, the backup-sheet thicknesses for the yield and fracture criteria can be plotted against particle diameter at a number of velocities. When this is done it is found that, for either criterion, t_b is approximately proportional to the cube of the particle diameter. Thus, under these conditions, Equation (3) indicates that v_i , the initial velocity of the loaded area, is roughly constant.

The Effect of Spacing

Spacings of 2.54, 5.08, and 10.16 cm were investigated for the Apollo particle (1.02-mm diameter) at 30.4 km/sec. The results for both the yield and fracture criteria show that the sheet thickness necessary for either decreases approximately with the inverse square of spacing. This result, plus those of the preceding sections, gives rise to an approximate equation for rear sheet thickness. For 7075-T6 aluminum this equation is given by

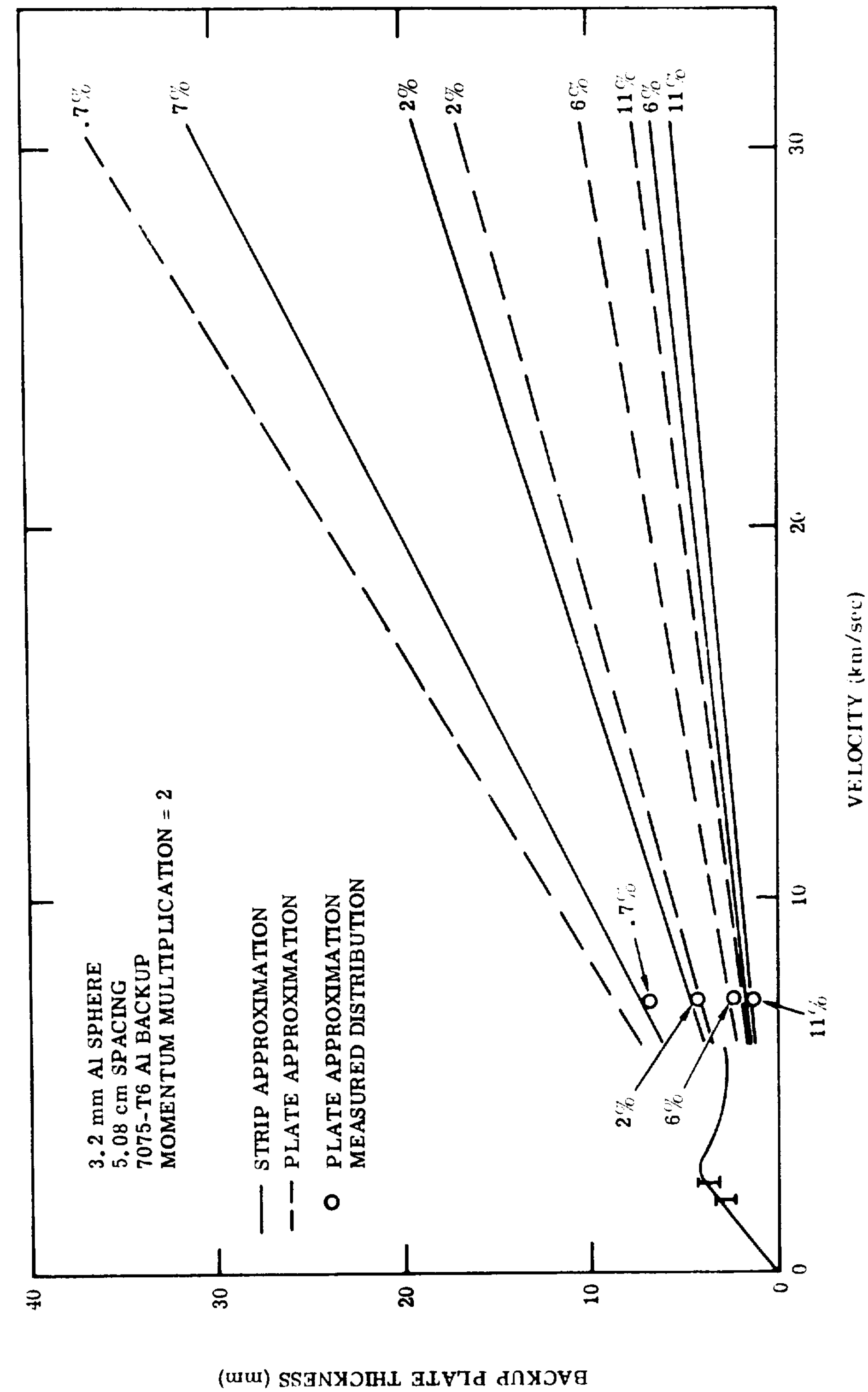

Figure 9(a) Comparison of Strip and Plate Calculations: 3.2-mm Aluminum Sphere

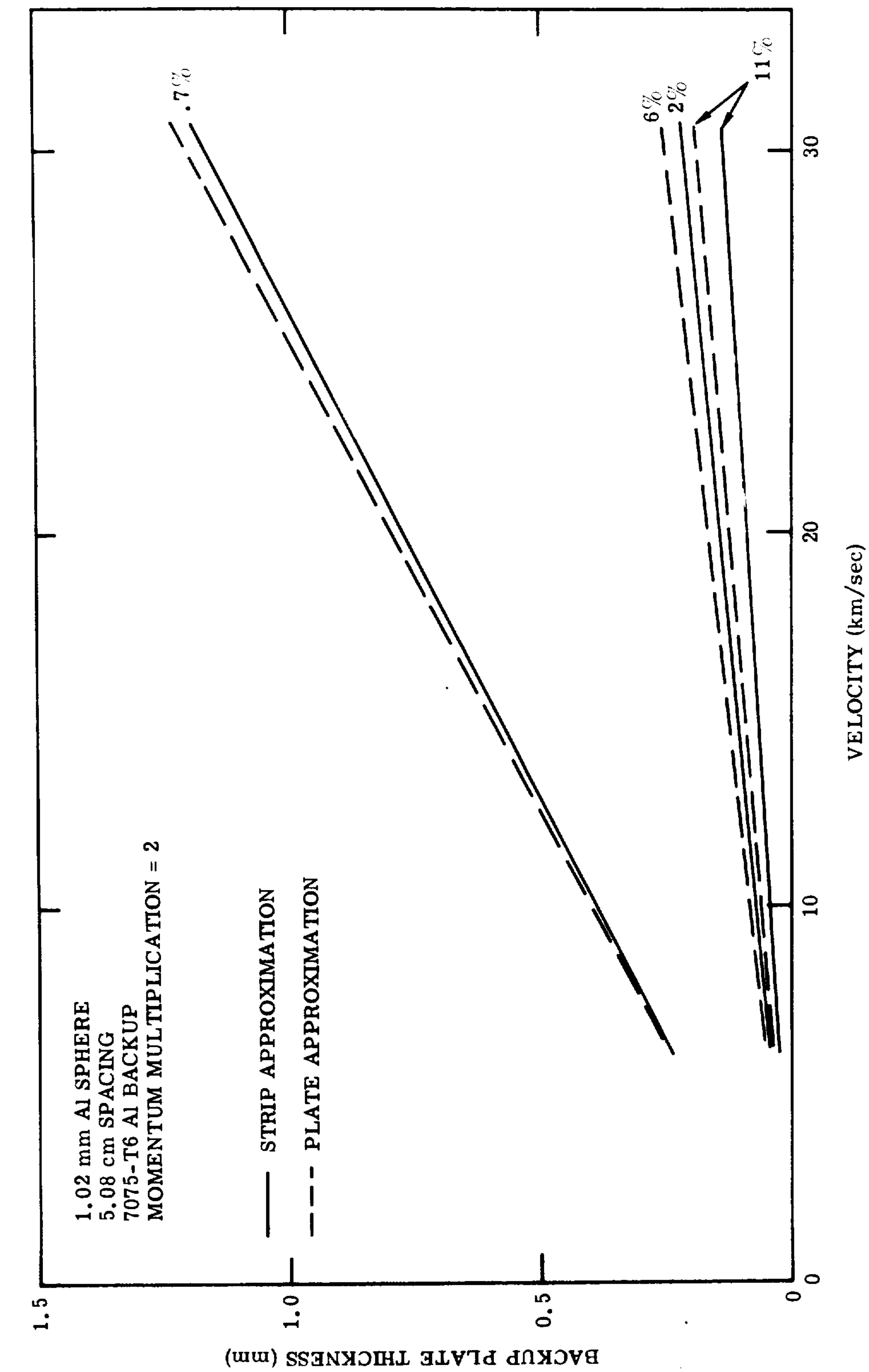

Figure 9(b) Comparison of Strip and Plate Calculations: Apollo Particle

$$t_b = C \frac{M_p V_p}{S^2} \quad (4)$$

where $C = 415 \pm 140$ and 82 ± 14 for the yield and fracture criteria, respectively, t_b is in millimeters, M_p is in grams, V_p is in km/sec, and S is in centimeters. (Note: because the exact solutions do not require v_i in Equation (3) to be exactly constant, there is not a constant value for C at a specific maximum strain.)

The Effect of Pre-Tensioning the Backup Sheet

In many space applications, the structure to be protected will be a pressurized fuel tank; hence, it was decided to investigate the effect of pre-tensioning the rear sheet (in one direction only). Since the computer code for the strip approximation can accommodate such pre-tensioning, solutions were obtained for a 1.02-mm particle at 30.4 km/sec with pre-tensioning of 25%, 50%, 75%, and 100% static yield stress. The centerline displacements against time are shown in Figure 10(a), which gives evidence that pre-tensioning can significantly decrease the deflection of the sheet. Also, the sheet thicknesses required for both the yield and fracture criteria are shown in Figure 10(b) . These results reveal that the thickness required for the yield criterion is not very sensitive to pre-tension, whereas the thickness based on the fracture criterion is sensitive to the amount of pre-tension.

Extensions of the Strip Approximation

The strip approximation has been shown to be in good agreement with experimental results; however, the complete solution should consider a centrally loaded circular plate. The numerical technique of Witmer, et al,[5] has been applied to the plate analysis and the results agree well with those from the strip approximation. Such comparisons are shown in Figures 9(a) and 9(b).

Note also that either the strip approximation or complete plate analysis can be used to analyze impacts in multi-sheet targets by summing the momentum in the loaded segment of a sheet at the time fracture occurs around the circumference

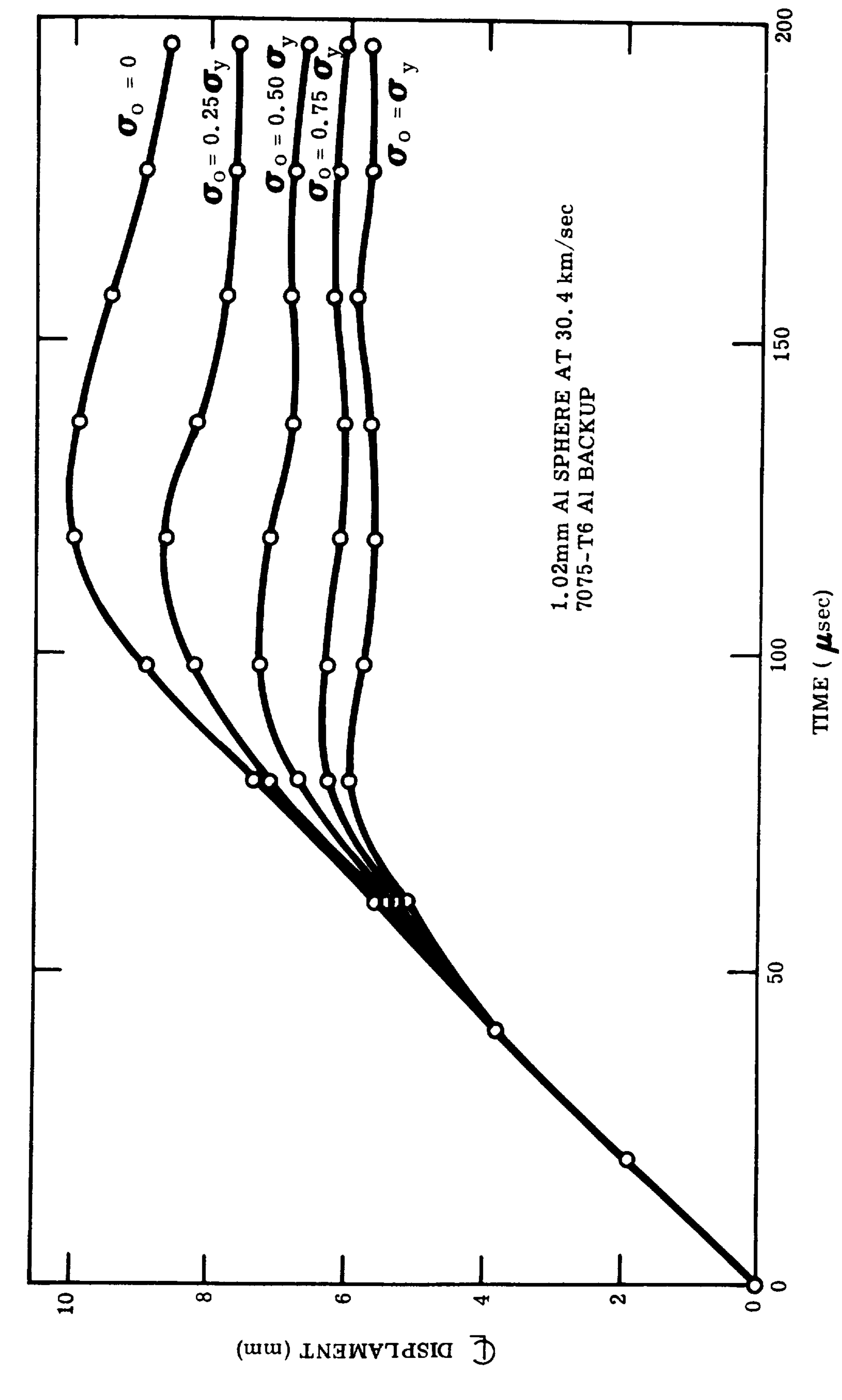

Figure 10(a) Pre-Tensioned Beam Behavior: Centerline Displacement vs Time

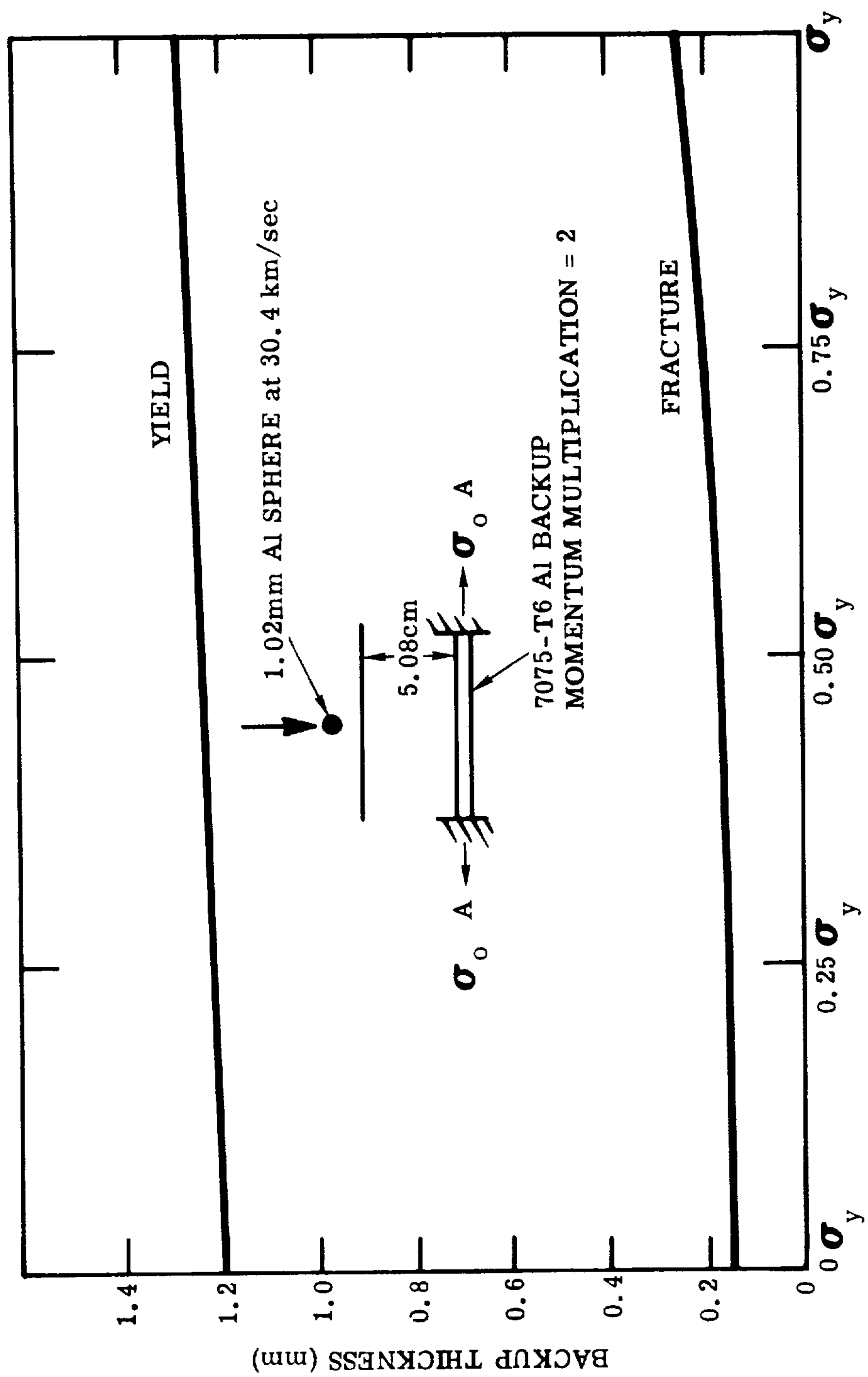

Figure 10(b) Pre-Tensioned Beam Behavior: Backup Thickness vs Pre-Tension Stress of the loaded area. This gives the momentum (reduced from twice the original particle momentum) to be applied to the next sheet in the array. The analysis is then continued until either a sheet is not perforated or the last sheet is reached.

INTERACTION OF DEBRIS WITH A SHIELDED TARGET – EXPERIMENTAL

Experimental studies in support of the theoretical studies described above have been performed with a light-gas gun at impact velocities up to eight kilometers per second. This section describes some of the results of these experiments. Appendix A presents the raw data from all the experiments performed to date.

Momentum Multiplication

Extensive experiments utilizing a ballistic pendulum[7] were carried out to measure the momentum transfer to the second sheet as a function of impact parameters. Initial experiments involved the measurement of momentum applied to the backup while varying the bumper thickness and the impact velocity in aluminum-aluminum impacts. The results of these experiments are summarized in Figure 11. The thin bumpers (0.305 mm, 0.635 mm and 1.02 mm) gave very similar results. The ratio of the measured momentum applied to the backup sheet divided by the incident momentum increased with velocity up to about 5 kilometers per second, then remained constant throughout the rest of the experimental range. The thicker shield, 1.6 mm, exhibited a continued increase in the momentum multiplication ratio throughout the experimental range. Since it has been argued that the momentum multiplication ratio for the thin-sheet impact case has an upper bound of 2.0 and semi-infinite impact has no upper bound[7] it is to be expected that the momentum multiplication ratio should show an increase for the thicker targets.

The momentum multiplication values presented in Figure 11 cover the range of solid debris impact through completely melted debris. There appears to be no sharp change in behavior in this transition, with perhaps the exception of a change of slope at about 5 kilometers per second corresponding to the onset of melting in aluminum-aluminum impact.

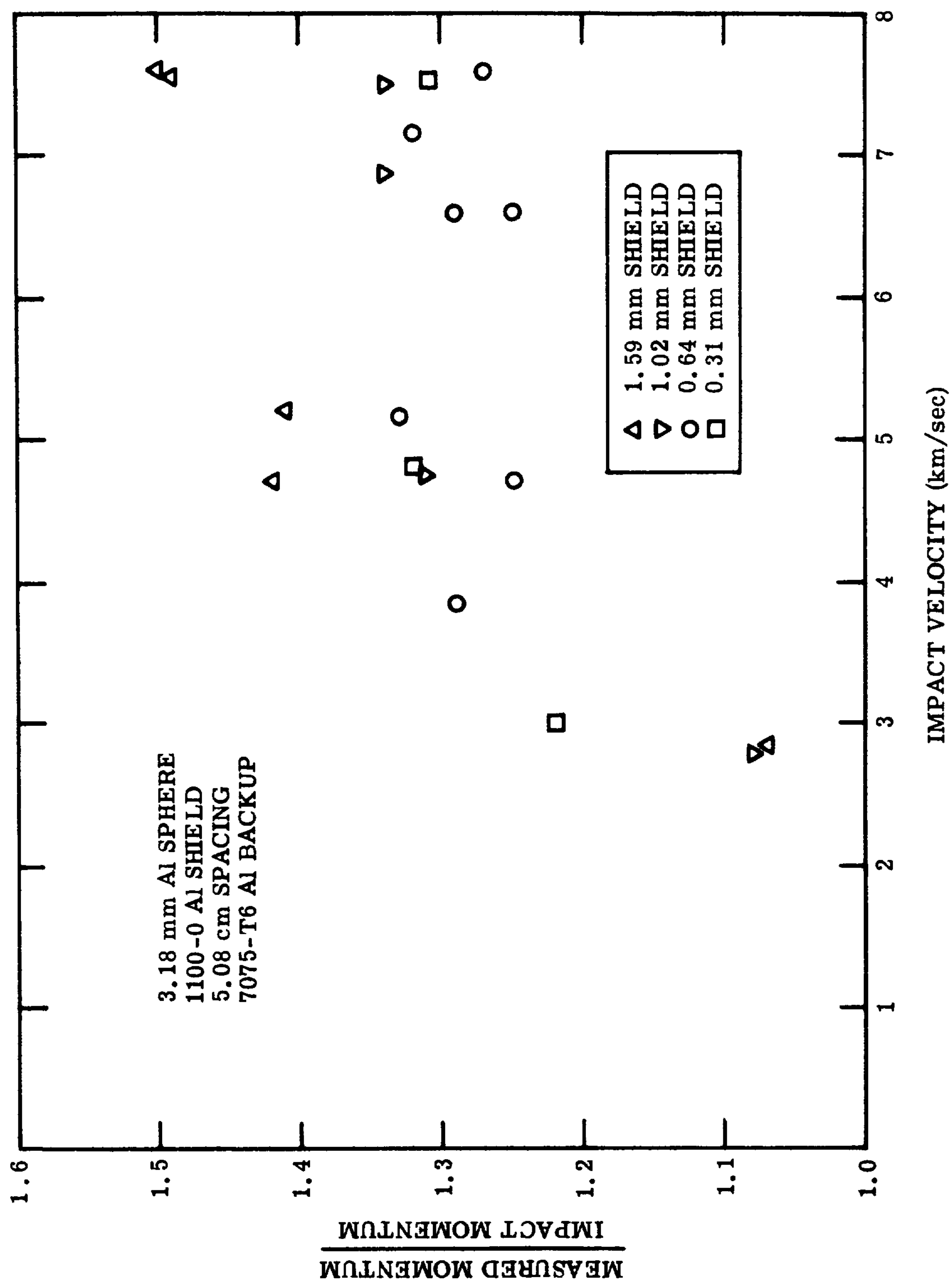

Figure 11 Momentum Multiplication vs Velocity

As a test of the effect of spacing upon the momentum multiplication ratio, experiments were conducted with spacings less than the 5.08-centimeter spacing of the previously described experiments. The values obtained in these experiments were identical, within the ± 4% error of the measurements, to the values obtained with the 5.08-centimeter spacing (Table I).

Table I
EFFECT OF SPACING

Shot No.	Shield Thickness (mm)	Impact Velocity	Spacing (cm)	Momentum Multiplication
D-1225	1.02	5.88	2.54	1.32
9996		6.46	1.27	1.30
1351		7.47	1.27	1.33
1352	0.64	7.07	1.27	1.35
3.18-mm Aluminum Spheres Impacting 1100-0 Aluminum Shields				

On the basis of these experiments it is concluded that spacing has no effect on momentum transfer.

The value of the momentum multiplication factor attained for the aluminum-aluminum thin-sheet impact case was much less in the case of the three thinnest shields than the value of 2.0 postulated as the upper bound. The aluminum-aluminum impact represented a liquid debris impact and it was felt that perhaps the impact of vapor debris would more closely approach the value of 2.0. Experiments were performed with cadmium projectiles and shields in which the debris striking the backup sheet was in vapor form. The results of these experiments are shown in Table II. As can be seen, the values attained are again much less than 2.0.

The experiments performed with 0.64-mm shields represented a transition from liquid debris striking the backup (the test at 3.18 kilometers per second) to vapor debris. The value of the momentum multiplication ratio reached a value of 1.4 at 5.38 kilometers per second and remained unchanged throughout the experimental range. The experiments performed with the 0.33-mm shields covered the transition from solid debris to liquid debris. Again the highest value attained is far less than 2.0.

Table II
CADMIUM-CADMIUM IMPACTS

Shot No.	Shield Thickness (mm)	Impact Velocity (km/sec)	Momentum Multiplication
D-1046	0.64	3.18	1.21
1324	↓	5.38	1.41
1327	↓	5.76	1.38
1045	↓	6.40	1.42
1454	↓	6.40	1.39
1230	0.33	3.60	1.26
1463	↓	5.18	1.28
1019	↓	5.61	1.34
3.18-mm Cadmium Spheres			

The attainment of values for the momentum multiplication ratio of less than 2.0 can be accounted for by a probable lack of perfectly elastic vapor impact with the backup sheet and the spread of the debris before striking the backup sheet, resulting in non-normal impacts.

LOW DENSITY PROJECTILES: Two sets of experiments were performed using low density materials for projectiles. The first series was performed using Inlyte as the projectile material. This is composed of very small glass spheres held together in a plastic matrix. The projectiles used had a bulk density of 0.7 grams per cubic centimeter. The values of the momentum multiplication factors obtained for impacts against aluminum shields (Table III) are in agreement with those obtained for aluminum-aluminum impacts. An examination of the backup sheet shows that the damage was due to shield fragments and there was no evidence of melting of the aluminum.

The second set of momentum-transfer experiments with low-density projectiles was performed using nylon as the projectile material. The nylon had a density of

1.15 grams per cubic centimeter. In contrast to the momentum multiplication factors obtained using Inlyte as the projectile material, the momentum multiplication was quite high (Table III). The damage suffered by the backup was very similar to that obtained with the Inlyte projectiles, with a great number of small craters apparently caused by shield fragments. With the nylon, as with the Inlyte, there was no evidence of melted aluminum on the backup target. Because there is no apparent difference in the damage to the backup sheets it must be concluded that the difference in the values of the measured momentum transfer must be due to differing projectile properties.

Table III
LOW-DENSITY IMPACTS

Shot No.	Projectile	Shield Thickness (mm)	Impact Velocity (km/sec)	Momentum Multiplication
D-1391	4.90-mm Inlyte	0.64	4.69	1.20
1394	↓	0.64	7.91	1.24
1393	↓	0.305	4.68	1.25
1349	4.19-mm Nylon	1.02	6.31	1.55
1371	↓	1.02	7.13	1.50

Shields 1100-0 Aluminum, 5.08-cm spacing, 7075-T6 Aluminum Backups

DISTRIBUTION OF MOMENTUM: A double ballistic-pendulum arrangement was used to measure the distribution of momentum applied to a shielded target. The experimental arrangement was such that the momentum felt by a variable-size central circular area of the target was measured by one pendulum, and the momentum applied outside this central area was measured by another pendulum. In this study the projectiles were 3.2-mm aluminum spheres at 7.3 km/sec, the shields were 0.64-mm 1100-0 aluminum, and the spacing was 5.08 cm.

The results of the tests are shown in Figure 12. It is seen that the assumed distribution and experiment differ, hence it was decided to investigate the sensitivity of the rear-sheet analysis to momentum distribution. This was done by calculating the rear-sheet thickness necessary for the experimental conditions

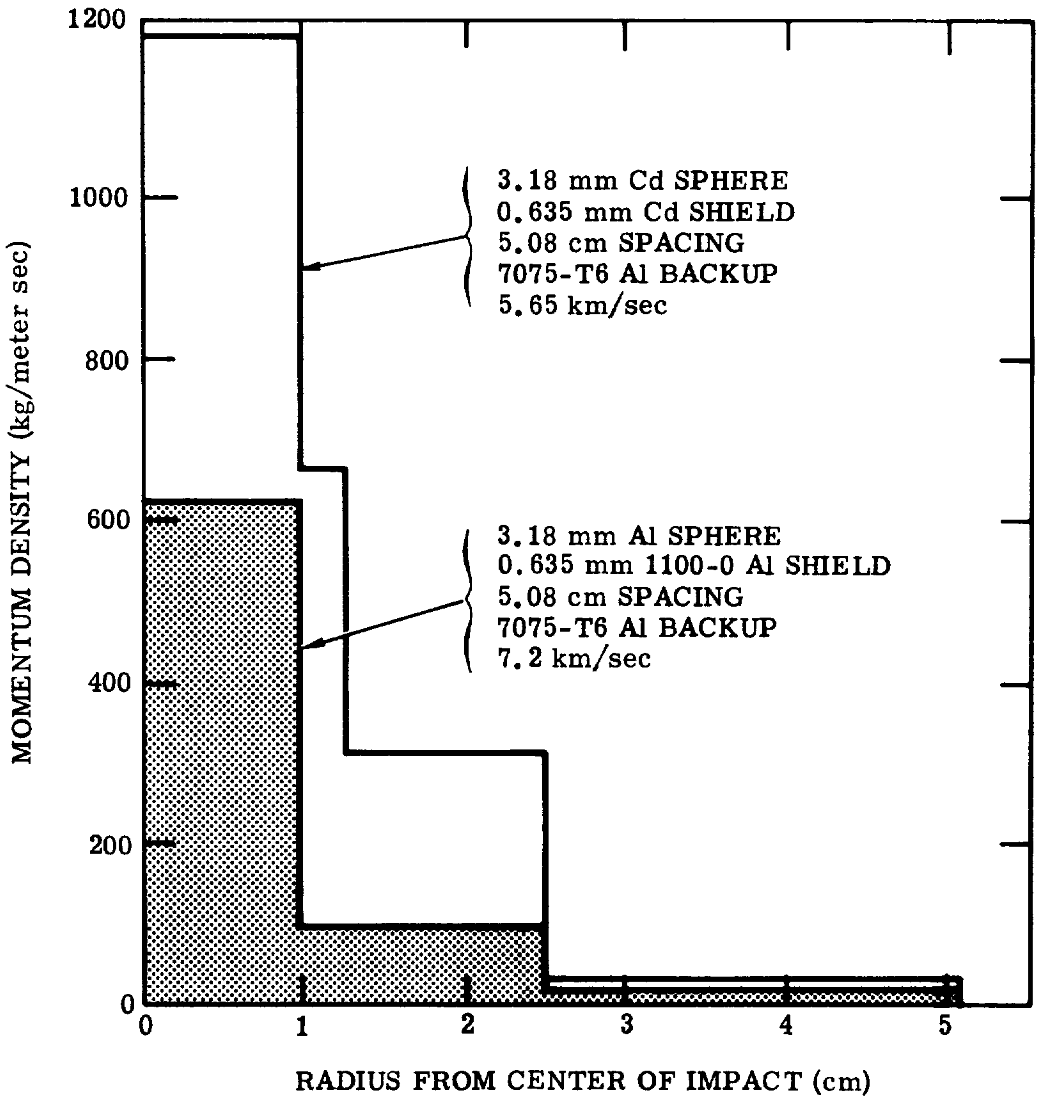

Figure 12 Momentum Distribution

relevant to Figure 12, and for the measured momentum distribution. The results of the analysis, presented in Figure 9(a), indicate that the predicted thicknesses are not radically altered by the changes in momentum distribution.

Also shown in Figure 12 is the distribution obtained with cadmium-cadmium impacts. The distribution of the cadmium momentum is less peaked than the aluminum-aluminum distribution. The aluminum debris was in molten form while the cadmium debris was vaporized, and this may account for the flatter cadmium distribution. (It should be noted that the cadmium projectiles had a mass of 0.145 grams while the aluminum projectiles had a mass of 0.047 grams; thus the cadmium momentum and momentum density is greater than the aluminum. The portion of the momentum near the center is less for the cadmium.)

Multi-Sheet Structures

The question of the effectiveness of single versus multiple backup sheets was approached by approximating the failure of the backup sheet with the strip approximation. When fracture occurs in any of the six layers of the strip, the momentum of the broken segment of the strip is summed. The result of this procedure is shown in Figure 13. The results indicate that the use of multiple sheets offers little or no advantage over single backup sheets, as there is no significant decrease in the momentum through the second sheet until it has a thickness of approximately 90% of the fracture thickness.

A series of experiments was conducted to test the validity of this approach. The first three experiments utilized the ballistic pendulum behind various thicknesses of second sheet to attempt to measure the momentum delivered through the second sheet. The results of these tests are summarized in Table IV.

The poor agreement between the experiments and the predictions is due in part to spall from the second sheet and also to the momentum multiplication in the catch material on the ballistic pendulum.

TR65-48

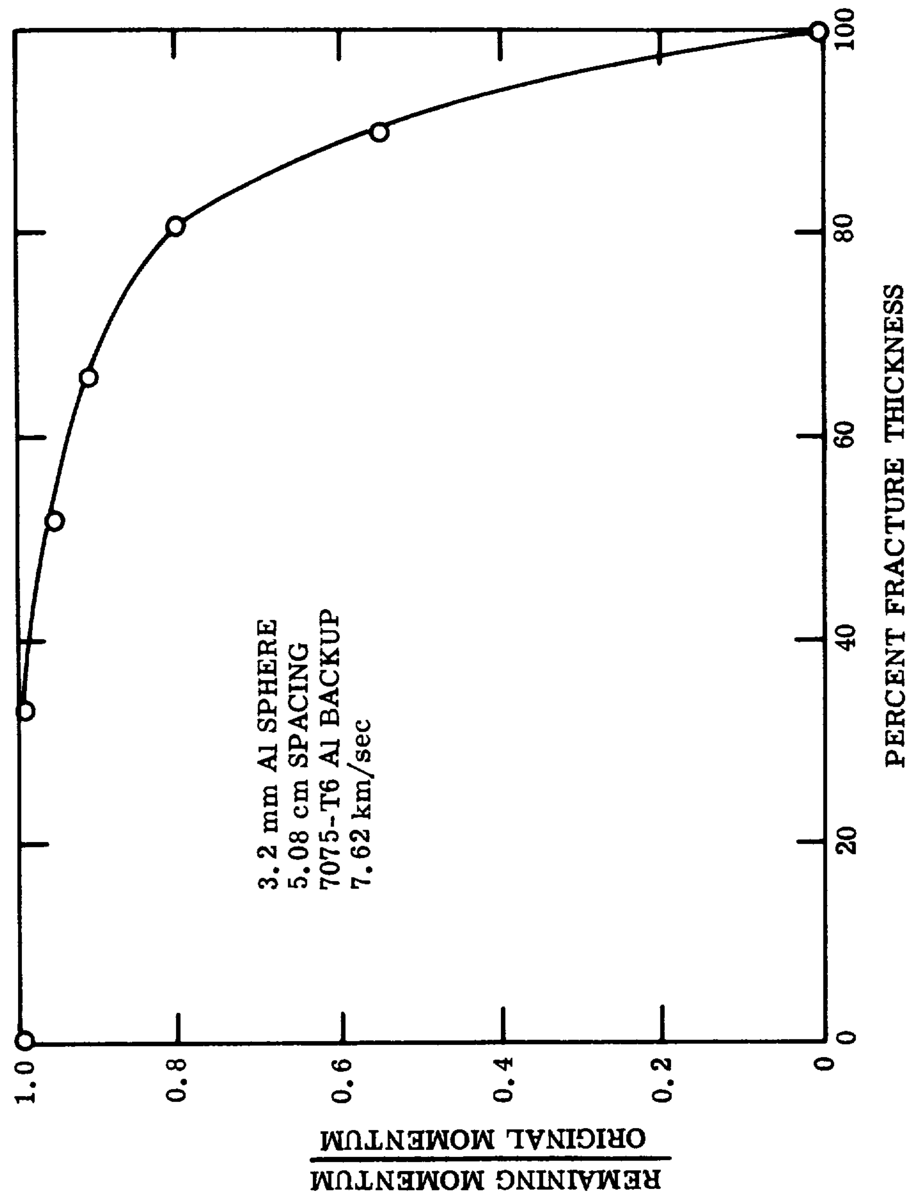

Figure 13 Remaining Momentum vs Backup Thickness

Table IV MOMENTUM THROUGH BACKUP			
Shot Number	D-1437	1400	1442
Velocity	8.05 km/sec	7.60	7.50
% of Fracture Thickness	32	50	100
Momentum Through Backup (Actual)	1.38	0.65	0.47
Momentum Through Backup (Predicted)	0.99	0.95	0
All tests 3.18-mm aluminum spheres, 5.08-cm spacing, 7075-T6 aluminum backups.			

A series of experiments was then undertaken with actual spaced multiple sheets. The first test was against a double-sheet structure, bumper and backup (see Table V). The damage in this case was minor fracture and spall. This structure corresponds to the fracture case calculated with the plate approximation and measured momentum distribution shown in Figure 9(b). The second test was conducted against a three-sheet structure (see Table IV). The damage in this case consisted of complete fracture failure of the second sheet, but only yield to the third sheet. The last test consisted of an impact against a four-sheet structure, again of the same areal density as the double-sheet structure. In this instance the second sheet again suffered a complete fracture failure and in this case the third sheet was perforated by what appeared to be fragments of the second sheet. The fourth sheet was essentially undamaged.

Table V MULTI-SHEET IMPACTS			
Shot No.	D-1442	D-1449	D-1450
Velocity	7.50 km/sec	8.14 km/sec	7.93 km/sec
First Sheet	0.64 mm	0.64 mm	0.64 mm
Spacing	5.08 cm	5.08 cm	5.08 cm
Second Sheet	1.27 mm	0.64 mm	0.41 mm
Spacing	--	5.08 cm	5.08 cm
Third Sheet	--	0.64 mm	0.41 mm
Spacing	--	--	5.08 cm
Fourth Sheet	--	--	0.41 mm
Last Sheet Perforated	Second	Second	Third
3.18-mm Aluminum Spheres			
All First Sheets: 1100-0 Al All Other Sheets: 7075-T6 Al			

On the basis of the two sets of experiments, it was felt that the strip approximation was not adequate. The analysis is presently being modified such that fracture must occur in all six layers before the momentum is summed. Also, the impact of sheets after the second does not appear to be a blast-loading phenomenon but a fragment-impact process. The description of the momentum through the second sheet may not provide a complete description of damage to the following sheets.

Fillers

Preliminary experiments have been made on the effectiveness of filler materials upon reduction of damage in bumper-protected structures. Experiments were originally conducted with the ballistic pendulum to determine the momentum transfer through the foam material, in this case styrofoam. The ballistic pendulum record indicated that the momentum transfer was very large to the second sheet and, in fact, exceeded the capacity of the pendulum.

An experiment was performed in which the foam material was placed between the first and second sheet and the second sheet thickness made such that the areal density would match that of test number D-1441 (see Table V). The impact of this target with a 3.18-mm aluminum sphere at 7.56 kilometers per second resulted in the removal of all the filler material from between the bumper and backup and severe deformation of both the backup and the bumper. The structure was not perforated. For these particular test conditions, this particular filler provides more protection than the bumper-backup combination of the same weight. The foam used was a closed-cell foam and this construction may contribute to the deformation of the shield and backup through shock transmission. Further experiments will be performed to evaluate the usefulness of foams, investigating the effects of open and closed cells, density and foam composition.

Experimental Check of Predictions for a 1.02-mm Aluminum Particle at 30.4 km/sec

Several experiments were conducted to check the validity of the calculation shown in Figure 8(c) for a particle with a diameter of 1.02 mm (Apollo) at 30.4 km/sec. The momentum of this particle at 30.4 km/sec is nearly the same as a particle

1.6mm Al SPHERE AT 7.88 km/sec
0.305mm 1100-0 Al SHIELDS
5.08cm SPACING
7075-T6 Al BACKUP

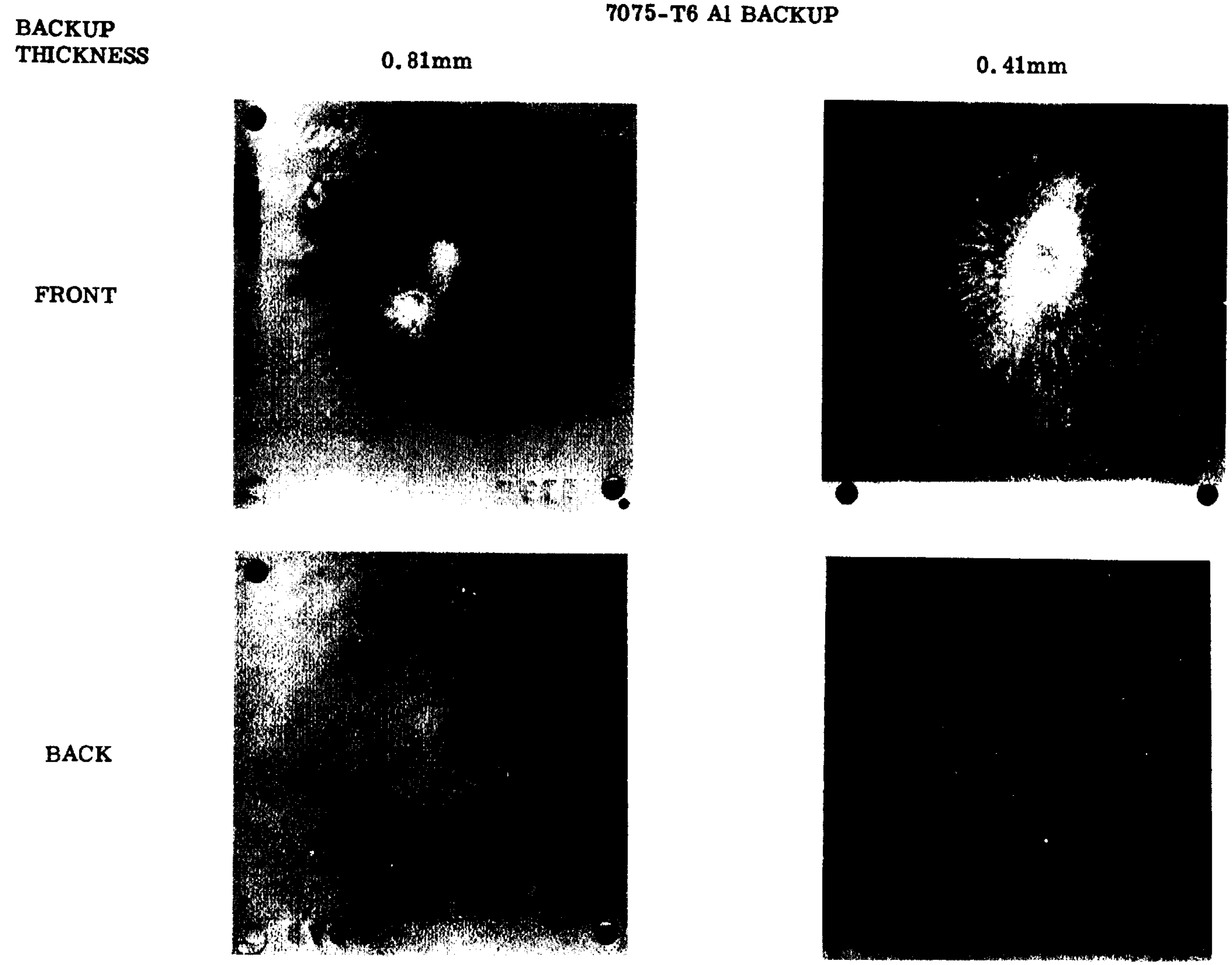

Figure 14 Backup Targets – Simulated Apollo Impacts

with a diameter of 1.6 mm at 7.8 km/sec. Assuming the momentum multiplication factor to be the same at both velocities, a 1.6-mm-diameter particle at 7.8 km/sec can simulate the backup sheet loading from the Apollo particle at 30.4 km/sec. For this reason tests have been conducted with 1.6-mm aluminum particles at 7.8 km/sec, spacing of 5.08 cm, 0.31-mm shields of 1100-0 aluminum (near optimum), and 7075-T6 aluminum backup sheets, 0.41, 0.82, and 1.64-mm thick. Photographs of the two thinnest backup sheets (Figure 14) show that neither failed due to impact. This is consistent with the results of Figure 9(b), where it is predicted that a 1.02-mm aluminum projectile should not fracture such sheets at 30.4 km/sec. Also consistent with the predictions of Figure 9(b) is the lack of any deformation of the 1.64-mm backup sheet (not shown in Figure 14).

DISCUSSION

SPALLING

As mentioned earlier in this report, the impulsive load applied to a shielded target can cause spallation as well as gross deformation. The study of spallation has only recently commenced at GM DRL; however, some preliminary results are worth reporting. These results have been obtained by idealizing the impulsive load applied to the rear sheet, and then using a one-dimensional elastic-plastic wave analysis (GM DRL computer program MATERIALS I).

The spall-producing load applied to a shielded target has been approximated by the plate impact illustrated in the upper right-hand corner of Figure 15. The assumed plate impacts at the projectile velocity V_o , has a diameter of $S/2$, and has the same mass and density as the impacting projectile. In addition, the plate material is assumed to behave as a fluid. The above assumptions seem reasonable in view of the following facts:

(a) X-rays from Reference 1 show that the majority of debris passing through a thin shield is near the front of the bubble and travels at approximately the impact velocity.

(b) At high velocity the debris is expected to have negligible strength (and behave as a fluid) due to shock-heating effects.

(c) Earlier results have shown that a spread of $S/2$ for the loading is reasonable.

Details of the stress waves produced in the rear sheet due to the above one-dimensional impact can be obtained from the GM DRL MATERIALS I code. This code has been obtained by writing the one-dimensional field equations, together with the constitutive equation, in finite difference form.[8, 9]

The constitutive equation for the elastic-perfectly plastic material subject to large compressions is based on the following assumptions:

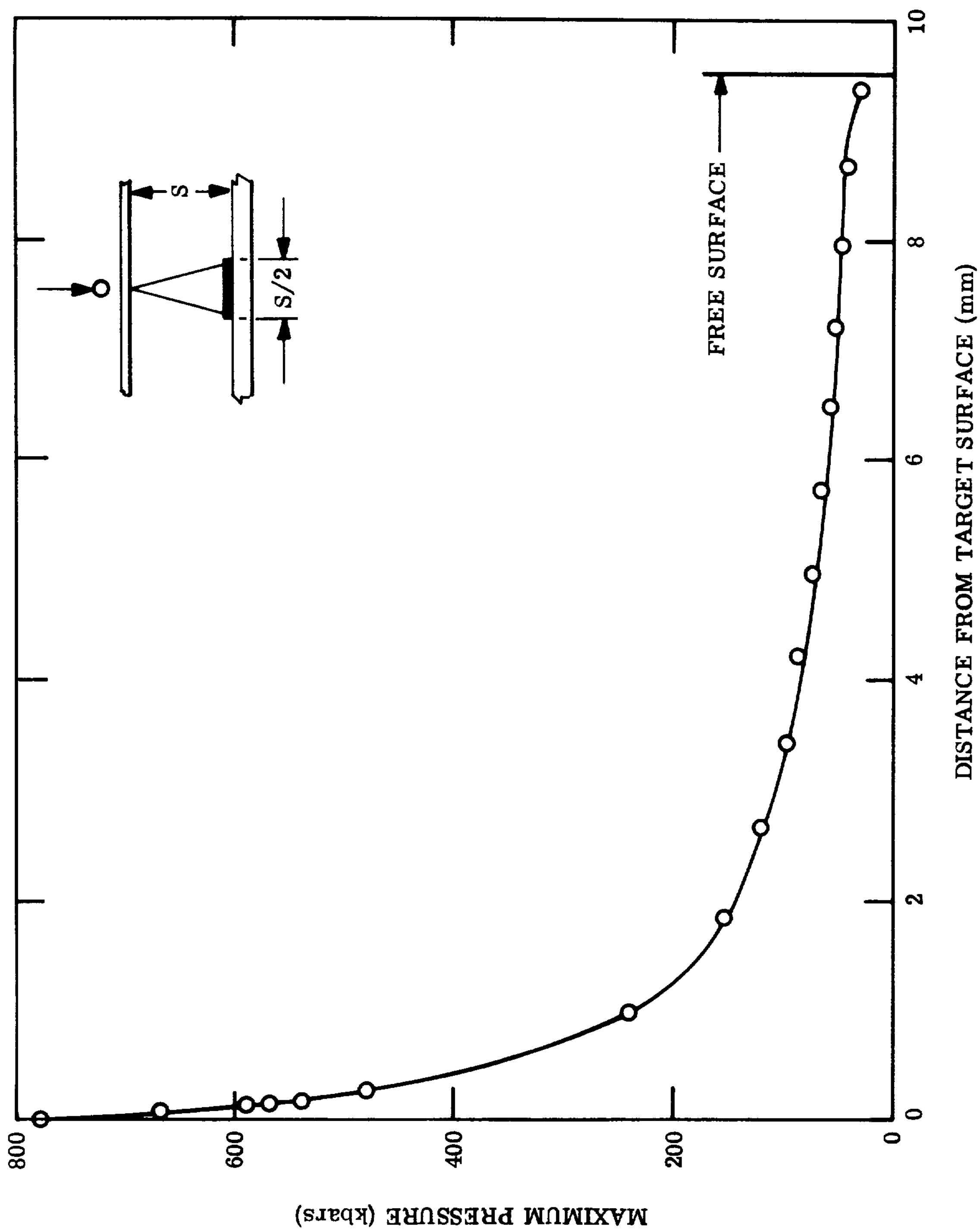

Figure 15 Maximum Pressure vs Distance

(a) The stretching can be expressed as the sum of elastic and plastic components.

(b) The spherical stretching follows the hydrodynamic equation of state and is entirely recoverable.

(c) The deviatoric stresses are subject to the Von Mises yield criterion.

Note that, in the analysis, only the flow in the rear sheet includes strength effects, whereas the flow in the impacting plate is assumed to be purely hydrodynamic.

To investigate the above analysis, computer calculations were performed to compare with the experimental conditions pertinent to Figure 4. The predicted plot of maximum pressure against distance into the target plate is shown in Figure 15. For a spalling stress of 13.5 kbar,[10] and taking into account the shape of the wave in the target, incipient spall is predicted in a target approximately 1-cm thick. This prediction is in good agreement with experimental results which show that a 0.96-cm-thick target just spalls, whereas a 1.27-cm target does not spall. Note also that a comparison of the results of Figures 4 and 15 indicates that a peak pressure of about 100 kbar is necessary for complete spall detachment.

The above good agreement between theory and experiment is considered to justify application of the technique to the case of 1.02-mm Apollo particle impacting a shielded structure.

LOW-VELOCITY IMPACT

The predictions of rear-sheet thickness made earlier in this paper have assumed that the debris passing through the bumper essentially blast-loads the rear sheet. This assumption is only valid at high velocities where the debris consists of very small particles. For an aluminum projectile impacting an aluminum shield it is safe to say that this condition is achieved when the debris contains some molten debris, i.e., above 7 km/sec. At lower velocities than this, incomplete fragmentation of the projectile occurs and the large fragments passing through the bumper can inflict substantial damage on the rear sheet.

To further investigate this effect, several tests were conducted using 3.2-mm aluminum projectiles, 0.64-mm (near optimum) shields of 1100-0 aluminum, 5.08-cm spacings, velocities from zero to 6.5 km/sec, and 7075-T6 backup sheets of various thicknesses. From these tests the rear-sheet thicknesses necessary to prevent spall detachment at various velocities were established, and the results are presented in Figure 16 (also in Figure 9(a)). It is seen that the thickness necessary rises to a peak at about 2.5 km/sec and then decreases as greater fragmentation of the projectile occurs. Note that the thickness necessary to stop such a particle at 2.5 km/sec is sufficient to stop the same particle at all velocities up to about 20 km/sec. Note also that the maximum penetration in Figure 16 is expected to be essentially independent of spacing, and scales approximately with projectile diameter.

NON-OPTIMUM SHIELDS

The previous section has pointed out that the assumption of blast loading of the backup sheet is invalid at low velocities. It is also invalid at high velocities if the shield is less, or significantly greater, than the optimum thickness given by Figure 3. In both cases the fragments impacting the backup sheet can be large and may cause significant cratering.

The non-optimum shield situation was experimentally investigated using 3.2-mm aluminum projectiles, 5.08-cm spacing, a velocity of 7.5 km/sec, and various thickness shields and backups of 7075-T6 aluminum. The damage inflicted upon 1.6-mm-thick backup targets in these tests is shown in Figures 17(a) and 17(b). The results of all the tests can be conveniently summarized in the solid line construction of Figure 17(c). Straight lines have been drawn between known points A, B, and C, where t_A (thickness at point A) corresponds to the thickness of rear sheet necessary to prevent spall detachment with no shield; t_B (thickness at point B) is the total thickness of structure to give 4% maximum strain (from Figure 9(a)) at optimum shield thickness of $t_s/d = 0.15$, and $t_C = t_A$ is the thickness of shield necessary to prevent spall detachment and thus require no backup sheet. The experimental results indicate that, for design purposes, if the structure is designed above ABC then no perforation of the rear sheet will occur. Note that, at a given velocity, thickness $t_A = t_C$ scales approximately as particle diameter d, whereas t_B scales as d^3.

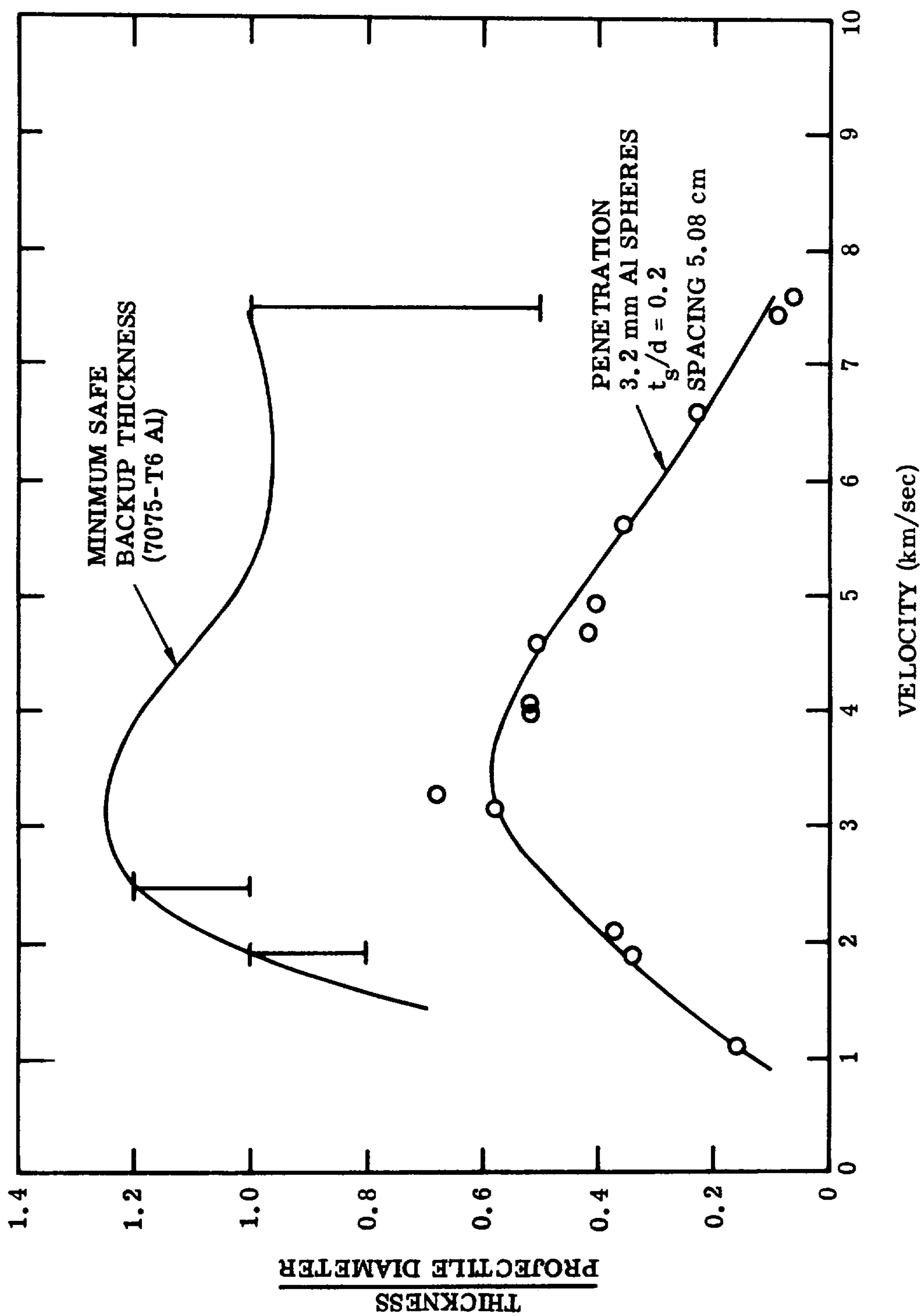

Figure 16 Backup Thickness Necessary to Prevent Perforation

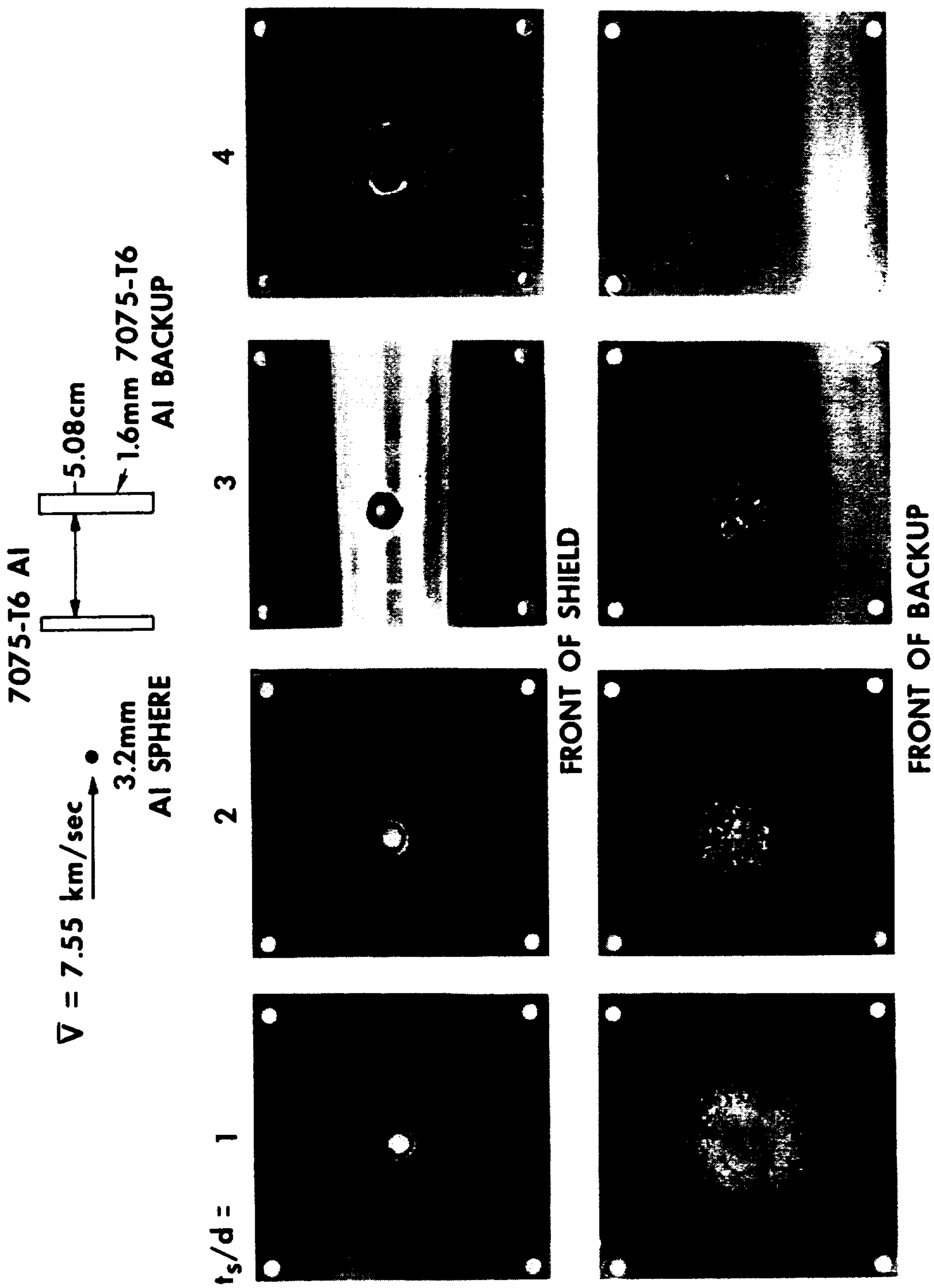

Figure 17(a) Non-Optimum Shield Data: Greater than Optimum Shields – Front of Targets

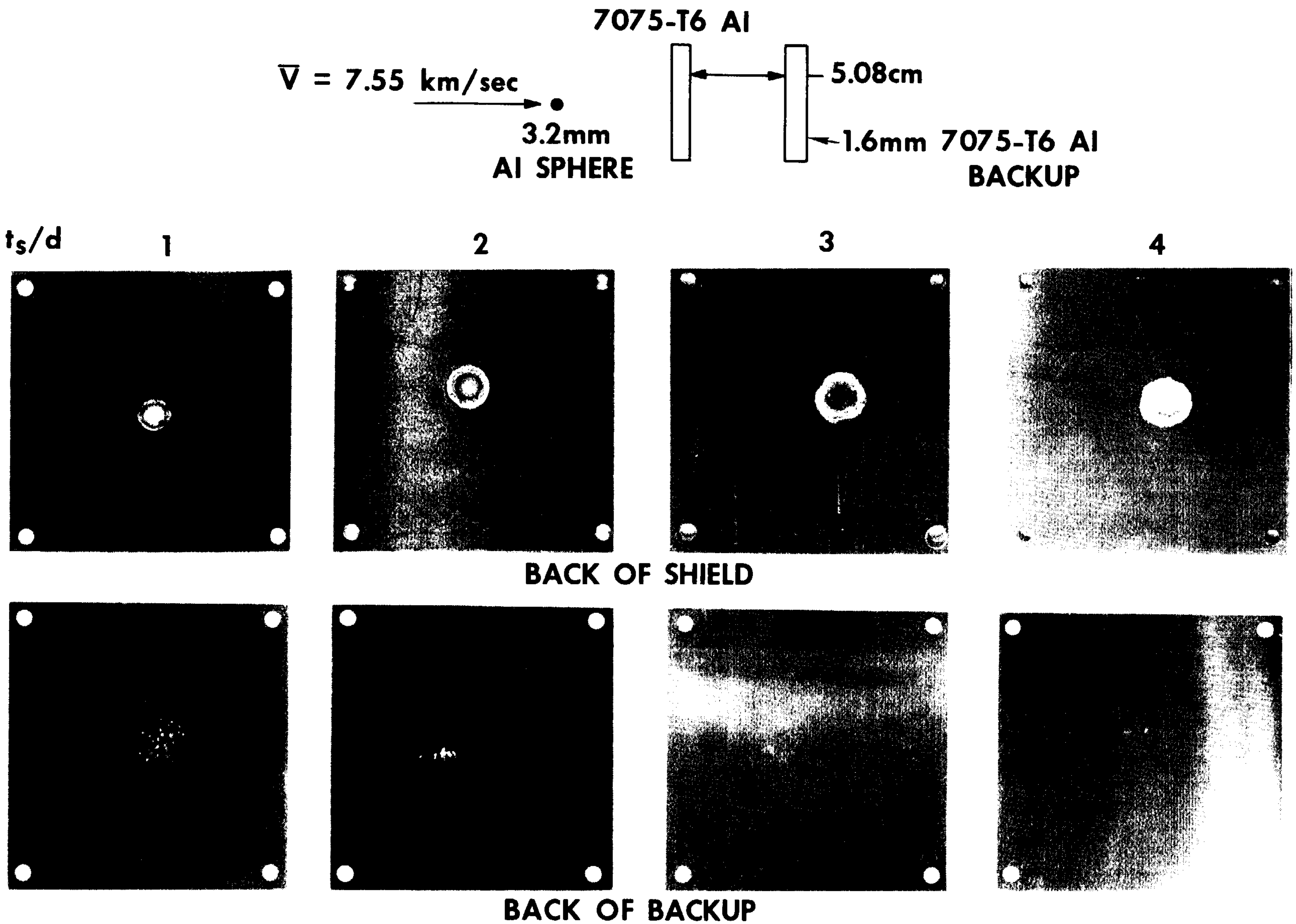

Figure 17(b) Non-Optimum Shield Data" Greater than Optimum Shields – Back of Targets

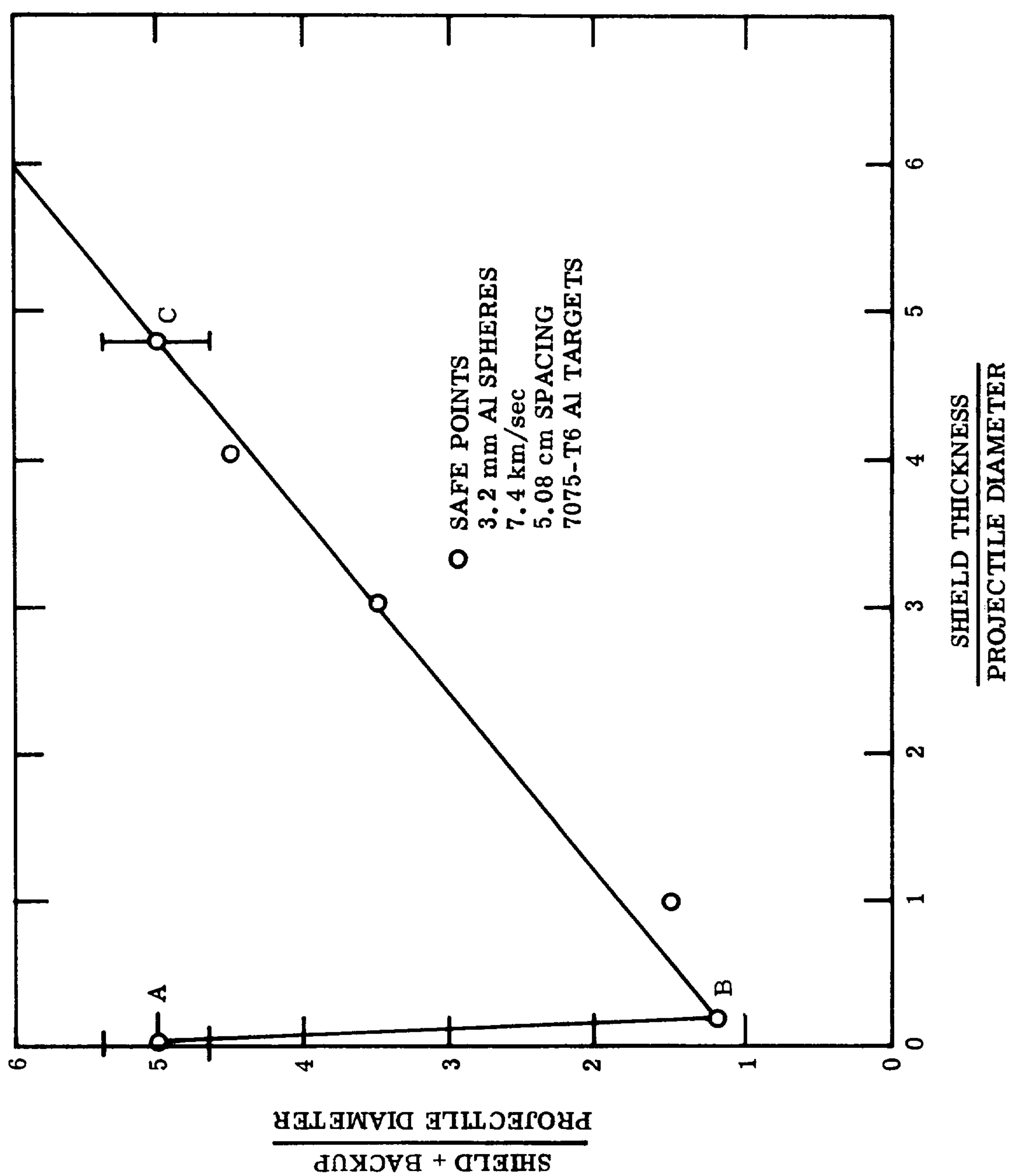

Figure 17(c) Non-Optimum Shield Data: Safe Thickness vs Shield Thickness

CONCLUSIONS

The large dynamic deformation analysis used to predict backup-sheet thicknesses has been found to give answers that are in good agreement with experimental results. In addition, preliminary predictions of spallation damage to a backup sheet seem to have validity. The greatest uncertainty in both the above analyses is in the assumed loading applied to the backup sheet.

The interest in Project Apollo makes it pertinent to summarize the conclusions regarding the optimum shielding requirements for this mission. The critical meteoroid mass was shown earlier to be the same as that of a 1.02-mm-diameter aluminum sphere, and Figure 3 shows that for this particle a 0.20-mm aluminum shield ($t_s/d = 0.19$) will be adequate at velocities above 7 km/sec. Figure 9(b) shows also that, for a spacing of 5.08 cm and a velocity of 30 km/sec, a 1.20-mm-thick backup sheet of 7075-T6 aluminum is not expected to yield. The final design check is to see if the above structure will resist perforation at velocities below 7 km/sec. This is determined from Figure 16, where it is seen that a maximum backup thickness of 1.30 mm ($t_b/d = 1.25$) is required at a velocity of 3 km/sec. Thus, for this particular mission the necessary thickness of total structure is 1.50 mm.

A final point of interest is that even though the optimum structural requirements of Apollo for meteoroid protection are modest, this will not always be the case. For example, Figure 3 shows that for a Mars mission, with the same vulnerable area and puncture probability as Apollo, the structure must be protected against a 0.125-gm meteoroid. Equation (3) shows that the backup-sheet thickness must be 170 times that required for Apollo. Of course, Equation (3) also shows that the way to decrease this weight is to increase the spacing.

REFERENCES

1. C. J. Maiden and A. R. McMillan, "An Investigation of the Protection Afforded a Spacecraft by the Thin Shield", AIAAJ, Vol. 2, No. 11, (1964), pp 1992–1998

2. C. J. Maiden, "Meteoroid Impact", Space Exploration, McGraw Hill Book Company, Inc., New York, 1964, pp 236–284

3. "Meteoroid Environment in Near Earth, Cislunar, and Near Lunar Space", NASA MSC Engineering Criteria Bulletin EC-1, 1963

4. J. S. Curtis, "An Accelerated Reservoir Light-Gas Gun", NASA TN D-1144, 1962

5. E. A. Witmer, H. A. Balmer, J. W. Leech, and T. H. H. Pian, "Large Dynamic Deformation of Beams, Rings, Plates, and Sheels", AIAA J, Vol. 1, No. 8, 1963, pp 1848

6. R. E. Sennett and D. Skaar, "STRUCTURES I – The Response of Beams and Rings to High-Intensity, Short-Duration Loading", GM Defense Research Laboratories Report, TR65-08, Feb 1965

7. C. L. Meyers and J. A. Charest, "Research in the Properties of Optimum Meteoroid Shields, GM Defense Research Laboratories Report, TR64-48, Sep 1964

8. M. L. Wilkins, "Calculation of Elastic-Plastic Flow", Lawrence Radiation Lab., UCRL-7322, 1963

9. W. Herrmann, "A Lagrangian Finite Difference Method for Two-Dimensional Motion Including Material Strength: AFWL Tech. Rept. No. WL-TR64-107, Nov 1964

10. J. A. Charest, Work in progress, to be published as GM Defense Research Laboratories Technical Report

APPENDIX

DATA SHEETS

SHOT NO.	PROJECTILE MATERIAL	DIAMETER (mm)	SHIELD MATERIAL	THICKNESS (mm)	SPACING (cm)	BACKUP MATERIAL	THICKNESS (mm)	VELOCITY (km/sec)	TOTAL PENETRATION (mm)	HOLE SIZE (mm)	SPRAY DIAMETER (mm)	SPRAY ANGLE	MV/mv	REMARKS
D-878	2017 AL	3.18	1100-0 AL	0.534	5.08	7075-T6 AL	3.18	7.68	0.96	6.1	102	90		
879							1.60	7.81	HOLE	—	94	86		PISTON HIT
880							0.813	8.08	HOLE	6.1	89	82.5		
901				0.635			12.7	—	—	—	—	—		NO IMPACT
902								7.46	.89	6.6	94	86		
903								7.29	.92	6.6	97	87.5		
904								7.60	.89	6.6	94	86	1.27	
905				1.02				7.80	1.07	9.2	89	82.5		
909								7.50	1.17	8.6	89	82.5	1.34	
910								2.78	2.02	6.1	51	53.5	1.08	
911								5.43	1.48	7.2	84	79		
912							6.35	4.76	1.76	7.4	79	76	1.31	
913				0.635				4.72	1.96	5.8	81	77	1.25	
914				0.305				4.82	2.49	4.6	86	80.5	1.32	
915				1.60				4.72	1.81	8.6	94	86	1.42	
916				0.305				2.91	2.90	4.1	56	58		
917				1.60				2.85	2.06	6.9	41	44	1.07	
918				0.635				3.78	2.32	5.8	76	74		SHEAR DISK HIT
919								6.28	1.32	6.1	97	87.5		
920				0.305				6.89	1.58	4.8	102	90		
921				1.60				5.18	1.83	9.2	74	72		
947				0.305				2.91	3.03	4.1	51	53.5		
948								7.56	.78	—	97	87.5		
949				1.60				—	—	—	—	—		NO IMPACT
950				0.635				3.99	3.31	6.1	89	82.5		
951								6.40	1.35	—	97	87.5		PISTON HIT
952				0.305				3.14	—	—	76	74		SHEAR DISK HIT

SHOT NO.	PROJECTILE MATERIAL	DIAMETER (mm)	SHIELD MATERIAL	THICKNESS (mm)	SPACING (cm)	BACKUP MATERIAL	THICKNESS (mm)	VELOCITY (km/sec)	TOTAL PENETRATION (mm)	HOLE SIZE (mm)	SPRAY DIAMETER (mm)	SPRAY ANGLE	MV/mv	REMARKS
D-972	2017 AL	1.60	1100-0 AL	0.305	5.08	7075-T6 AL	0.813	7.89	0.33	3.3	99	88.5		
973							0.407	7.78	.79	3.6	97	87.5		BACKUP BENT
974							1.60	7.78	.31	—	102	90		PISTON HIT
975							0.407	7.87	.36	3.6	89	82.5		
976		3.18		0.635			6.35	4.57	2.28	6.4	84	79		
977								6.61	1.35	7.1	102	90	1.29	
978				0.305				7.56	.71	—	97	87.5		PISTON HIT
979				1.60				7.56	1.64	10.9	89	82.5	1.49	
980				0.305				7.65	.84	5.3	97	87.5	1.31	
992								3.00	3.15	4.3	84	79	1.22	
993				0.635				3.87	2.32	5.8	74	72	1.29	
994	PYREX							3.63	1.14	5.8	89	82.5		
995								6.58	1.02	6.4	97	87.5	1.36	
996	2017 AL			1.02	1.27			6.46	2.26	8.4	25	27.5	1.30	
997				0.635	5.08			3.76	1.81	5.6	76	74		
998	Cd		Cd	0.330			12.7	2.94	—	4.6	99	88.5		SHEAR DISK HIT
999								5.34	.49	5.6	99	88.5		
1000								—	—	—	—	—		NO IMPACT
1012	1100-0 AL	4.12 x 4.14 CYLINDER	1100-0 AL	0.635				4.97	2.85	7.6	109	90.5		
1013								7.22	3.38	8.1	109	90.5	1.51	
1014								5.47	2.09	7.9	109	90.5		
1018	Cd	3.18	Cd	0.330				—	—	—	—	—		NO IMPACT
1019								5.61	.46	5.3	89	82.5	1.34	
1020								—	—	—	—	—		NO IMPACT
1021								—	—	—	—	—		NO IMPACT
1022								—	—	—	—	—		NO IMPACT

SHOT NO.	PROJECTILE MATERIAL	DIAMETER (mm)	SHIELD MATERIAL	THICKNESS (mm)	SPACING (cm)	BACKUP MATERIAL	THICKNESS (mm)	VELOCITY (km/sec)	TOTAL PENETRATION (mm)	HOLE SIZE (mm)	SPRAY DIAMETER (mm)	SPRAY ANGLE	MV/mv	REMARKS
D-1044	Cd	3.18	Cd	0.635	5.08	7075-T6	12.7	5.48	0.66	7.6	97	87°		
1045								6.40	.69	7.6	99	89	1.42	
1046								3.18	.86	7.0	91	83	1.21	
1047							6.35	6.49	.76	7.6	97	87		
1048		4.0		.762				3.44	.81	7.9	127	103		
1049		3.18		.635				6.46	.71	—	94	86		PISTON HIT
1050	Ti	2.62	1100-0	1.02				—	—	—	—	—		NO IMPACT
1051	Cu	2.08						4.17	3.30	5.1	86	81		
1052	Ti	2.62						3.49	2.92	5.1	76	74		
1053								7.25	2.03	—	89	83		PISTON HIT
1054	Cu	2.08						7.10	2.06	6.4	83	79		
1055	Al	3.05						7.16	1.04	9.4	95	86		
1056								3.62	1.40	7.1	66	66		
C-722		3.18		.635				7.93	.71	4.8	95	86		
723							4.75	7.41	.89	4.8	—	—		
725				1.02			.813	7.02	—	—	—	—		PISTON HIT
726								5.43	∞	7.9	—	—		
D-1114	NYLON	4.19					6.35	2.92	1.14	7.9	53	56		
1115								6.10	1.17	9.7	102	90		
1116								6.80	1.27	10.9	108	94		
1117	Al	3.18		.635			12.7	3.26	2.49	5.1	56	58		
1118								3.11	2.90	5.1	56	58		
1119								3.29	1.57	5.1	61	62		
1120								3.38	2.16	5.1	61	62		
1121								5.61	1.73	6.4	86	81		
1122								5.64	1.73	6.4	84	79		
23								5.61	1.65	6.4	85	80		

SHOT NO.	PROJECTILE MATERIAL	DIAMETER (mm)	SHIELD MATERIAL	THICKNESS (mm)	SPACING (cm)	BACKUP MATERIAL	THICKNESS (mm)	VELOCITY (km/sec)	TOTAL PENETRATION (mm)	HOLE SIZE (mm)	SPRAY DIAMETER (mm)	SPRAY ANGLE	MV/mv	REMARKS
D-1124	Al	3.18	1100-0	0.635	5.08	7075-T6	12.7	5.78	0.81	—	81	77°		PISTON HIT
1125								7.50	.84	6.6	76	74		
1126								—	—	—	—	—		NO IMPACT
1127								7.32	1.02	—	89	83		PISTON HIT
1128								7.29	.74	6.6	89	83		

SHOT NO.	PROJECTILE MATERIAL	DIAMETER (mm)	SHIELD MATERIAL	THICKNESS (mm)	SPACING (cm)	BACKUP MATERIAL	THICKNESS (mm)	VELOCITY (km/sec)	TOTAL PENETRATION (mm)	HOLE SIZE (mm)	SPRAY DIAMETER (mm)	SPRAY ANGLE	MV/mv	REMARKS
D-1153	Cd	2.56	Cd	0.635	5.08	7075-T6 Al	1.60	3.84	0.76	6.1	102	90		
1154		3.18		.330			12.7	3.69	.69	4.8	89	82		
1155				.635				5.12	.89	5.2	89	82		
1156				.330				3.87	.74	4.8	76	74		
1157	Al		1100-0 Al	1.02			6.35	6.89	1.19	8.1	102	90	1.34	
1222	Cd		Cd	.330				3.55	1.04	4.85	86	81		
1223				.635				5.12	.81	7.22	89	82		
1224	PYREX		1100-0 Al				6.35	4.92	1.65	5.68	89	82	1.23	
1225	Al			1.02	2.54		12.7	5.88	1.65	7.87	43	81	1.42	
1226			Cd	.330	1.27			6.10	1.09	5.89	36	109	1.40	
1227	Cd				5.08			—	—	—	—	—		NO LAUNCH
1228								—	—	—	—	—		NO LAUNCH
1229	1100-0 Al	4.12 x 4.14 CYLINDER	1100-0 Al	.635				5.61	2.13	7.97	109	94	1.28	
1230	Cd	3.18	Cd	.330				3.60	.66	4.62	99	89	1.26	
1231	Al	1.59	1100-0 Al	.305				4.36	1.04	2.8	61	62		
1232							3.18	6.16	.43	3.2	91	84		PISTON HIT
1233				.152				4.69	1.02	2.5	61	62		
1234								6.59	.89	—	84	79		PISTON HIT
1235				.305				6.50	.46	3.0	99	89	1.18	
1236		3.18		.635			12.7	6.61	1.19	6.50	99	89	1.25	
1237								7.10	1.14	6.63	98	87		SABOT HIT
1238								7.19	.97	6.60	99	89		
1239								7.19	1.14	6.65	98	87	1.32	
1240								—	—	—	—	—		NO LAUNCH
1241								7.38	1.25	6.63	94	86		SABOT HIT
1242								7.26	.89	6.63	94	86		PISTON HIT

SHOT NO.	PROJECTILE MATERIAL	DIAMETER (mm)	SHIELD MATERIAL	THICKNESS (mm)	SPACING (cm)	BACKUP MATERIAL	THICKNESS (mm)	VELOCITY (km/sec)	TOTAL PENETRATION (mm)	HOLE SIZE (mm)	SPRAY DIAMETER (mm)	SPRAY ANGLE	MV/mv	REMARKS
D-1307	Al	1.59	1100-0 Al	0.81	5.08	7075-T6 Al	0.40	—	—	—	—	—		No LAUNCH
1308								—	—	—	—	—		No LAUNCH
1314		3.18		9.52			6.35	7.59	9.52	14.5	—	—	1.27	
1315				3.18				—	—	—	—	—		No LAUNCH
1316				12.7				6.88	11.0	16.1	—	—		
1317				3.18				7.47	1.27	14.3	—	—		PISTON HIT
1318	Inlyte	6.35		1.02			12.7	7.26	3.02	11.2	140	108		PISTON HIT
1319	Al	3.18		9.52			1.59	7.38	9.52	14.4	—	—		
1320				3.18				7.41	+	14.5	63	64		PISTON HIT
1321				6.35			6.35	7.50	6.40	15.9	76	74		PISTON HIT
1323							1.59	7.47	+	15.8	76	74		PISTON HIT
1324	Cd		Cd	0.635			12.7	5.38	0.635	7.35	76	74	1.41	
1325								5.70	0.630	7.37	76	74		
1326								5.70	0.762	7.67	76	74		PISTON HIT
1327								5.76	0.630		76	74	1.38	
1328	Al		7075-T6 Al	3.18			1.59	7.50	+	11.7	76	74		PISTON HIT
1329				6.35				7.38	+	10.5	—	—		
1330				12.7				7.44	1.02	11.7	—	—		
1331				9.52				7.50	9.52	7.37				
1332				12.7				7.47	6.83	[illegible]				
1333			1100-0 Al	0.635	1.27		12.7	7.47	2.72	6.78	32	[illegible]		
1334					2.54			7.47	1.35		54	90		PISTON HIT
1335								7.32	1.55	6.78	76	74		PISTON HIT
1336					1.27			7.29	2.74	6.76	20	83		
1337	50% FOAM Ni	2.62		1.02	5.08		6.35	3.48	3.18	4.93	65	[illegible]		
1338	Al	3.18		0.635			9.52	7.53	1.19	6.48	102	90		
1344	50% FOAM Cu	2.62		1.02			12.7	3.29	0.238	4.99	57	[illegible]	[illegible]	

\+ BACKUP BENT

SHOT NO.	PROJECTILE MATERIAL	DIAMETER (mm)	SHIELD MATERIAL	THICKNESS (mm)	SPACING (cm)	BACKUP MATERIAL	THICKNESS (mm)	VELOCITY (km/sec)	TOTAL PENETRATION (mm)	HOLE SIZE (mm)	SPRAY DIAMETER (mm)	SPRAY ANGLE	MV/mv	REMARKS
D-1345	50% FOAM Cu	2.62	1100-0 Al	1.02	5.08	7075-T6 Al	12.7	5.15	2.34	5.82	76	74°	1.26	
1346	50% FOAM Ni							5.03	2.49	5.94	76	74	1.35	
1347								6.70	2.18	—	—	—		PISTON HIT
1348	Cu	2.08						7.10	2.01	6.58	—	—		PISTON HIT

SHOT NO.	PROJECTILE MATERIAL	DIAMETER (mm)	SHIELD MATERIAL	THICKNESS (mm)	SPACING (cm)	BACKUP MATERIAL	THICKNESS (mm)	VELOCITY (km/sec)	TOTAL PENETRATION (mm)	HOLE SIZE (mm)	SPRAY DIAMETER (mm)	SPRAY ANGLE	MV/mv	REMARKS
D-1349	NYLON	4.19	1100-O Al	1.02	5.08	7075-T6 Al	12.7	6.31	1.32	9.38	98	87°	1.55	
1350	Al	3.18			2.54			7.38	1.63	8.64	36	70		
1351					1.27			7.47	2.67	8.34	20	77	1.33	
1352				0.635				7.07	2.54	6.60	19	72	1.35	
1353			7075-T6 Al	14.6				7.56	6.53	11.7				
1366				15.7				7.53	6.45	13.7				
1367				6.35	5.08		3.18	—	—	—	—	—		NO LAUNCH
1368								7.65	6.78	10.8				
1369	Cu	2.08	1100-O Al	1.02			12.7	—	—	—	—	—		NO LAUNCH
1371	NYLON	4.19						7.13	1.30	9.65	114	96	1.51	
1384	Al	3.18		.635			0.635	7.77	—	—	—	—		PISTON HIT
1385				1.02			12.7	—	—	—	—	—		NO LAUNCH
1386				.635				7.43	—	—	—	—		PISTON HIT
1387							0.635	—	—	—	—	—		NO LAUNCH
1388							12.7	—	—	—	—	—		NO LAUNCH
1389								5.18	2.77	6.20	102	90	1.33	
1390						1100-O Al		7.68	1.12	6.79	102	90		PISTON HIT
1391	INLYTE	4.90				7075-T6 Al	6.35	4.69	1.12	7.32	112	95	1.20	
1392								7.89	1.70	7.80	—	—		PISTON HIT
1393				.305				4.68	0.74	6.04	89	82	1.25	
1394				.635				7.91	1.60	7.90	142	109	1.24	
1395				.305				—	—	—	—	—		NO LAUNCH
1396	Al	3.18		.635		1100-O Al	12.7	7.56	1.30	6.76	114	96	1.24	
1397				1.59		7075-T6 Al		7.62	2.13	10.9	89	82	1.50	
1398								5.21	[illegible].34	9.31	7[illegible]	70	1.41	
1399	INLYTE	4.90		.305			6.35	7.86	—	—	—			PISTON HIT
1400	Al	3.18		.635			0.635	7.49	PERFORATION	6.71	102	[illegible]		

SHOT NO.	PROJECTILE MATERIAL	DIAMETER (mm)	SHIELD MATERIAL	THICKNESS (mm)	SPACING (cm)	BACKUP MATERIAL	THICKNESS (mm)	VELOCITY (km/sec)	TOTAL PENETRATION (mm)	HOLE SIZE (mm)	SPRAY DIAMETER (mm)	SPRAY ANGLE	MV/mv	REMARKS
D-1401	Al	3.18	1100-0 Al	0.635	5.08	7075-T6 Al	12.7	7.32	—	—	—	—		SABOT HIT
1402									—	—	—	—		No LAUNCH
1403									—	—	—	—		No LAUNCH
1404								7.56	1.30	6.78	99	88		0.0312 GRAM/CM³ STYROFOAM BACK OF SHIELD
1405		1.59					0.406	7.78	—	—	—	—		PISTON HIT
1406								—	—	—	—	—		No LAUNCH
1407	Cd	3.18	Cd				12.7	—	—	—	—	—		No LAUNCH
1408								—	—	—	—	—		No LAUNCH
1409								—	—	—	—	—		No LAUNCH
1410								5.00	—	—	—	—		NO IMPACT
1411								—	—	—	—	—		No LAUNCH

SHOT NO.	PROJECTILE MATERIAL	DIAMETER (mm)	SHIELD MATERIAL	THICKNESS (mm)	SPACING (cm)	BACKUP MATERIAL	THICKNESS (mm)	VELOCITY (km/sec)	TOTAL PENETRATION (mm)	HOLE SIZE (mm)	SPRAY DIAMETER (mm)	SPRAY ANGLE	MV/mv	REMARKS
D-1449	2017 Al	3.18	1100-0 Al	0.635	5.08	7075-T6 Al	0.635	8.14	FIRST SHEET	6.81	102	90		2 - 0.635 mm BACKUPS SPACED 5.08 cm
1450							0.407	7.90	SECOND SHEET	6.93	102	90		3 - 0.407 mm BACKUPS SPACED 5.08 cm
1452	Cd		Cd	0.350			12.7	—	—	—	—	—		NO LAUNCH
1453								5.18	.508	5.41	102	90	1.28	
1454				0.635				6.46	.635	7.92	102	90	1.39	
1455								6.53	.635	8.03	102	90		
1456		2.56			15.2		1.59	4.27	.635	6.32	254	80		
1457		3.18			5.08		12.7	6.53	.635	7.59	102	90		
1458	2024-T3 Al	3.18x9.53 ROD	2024-T3 Al	1.59	10.2	2024-T3 Al	25.4	4.63	6.84	7.65	178	82	1.43	
1459		2.49x14.9 ROD						4.74	8.74	—	184	84		
1460		4.55x4.55 ROD						4.94	1.53	10.2	193	87	1.32	
1461		5.23						4.91	1.45	10.3	184	84	1.37	
1462		6.61x2.21 DISC						4.79	2.18	12.5	172	81	1.25	
1463	2017 Al	3.18	1100-0 Al	0.635	5.08	7075-T6 Al	0.635	7.59	—	—	—	—		SABOT HIT
1464								—	—	—	—	—		NO LAUNCH
1465								—	—	—	—	—		NO LAUNCH
1466							1.02	7.74	—	—	—	—		PISTON HIT
1467								—	—	—	—	—		NO LAUNCH
1468							0.635	7.56	*	6.76	—	—		SPACING FILLED WITH 0.03 GRAM/CM³ STYROFOAM
1473	2024-T3 Al	3.63x7.27 ROD	2024-T3 Al	1.59	10.2	2024-T3 Al	25.4	3.87	4.25	7.90	152	74		
1474								5.40	5.03	8.19	184	84	1.43	
1475								2.93	3.18	7.27	133	67	1.26	
1476								6.10	4.55	9.48	184	84	1.39	
1477		2.11x21.1 ROD						4.45	17.2	5.8	152	74		

* SHIELD AND BACKUP BENT

SHOT NO.	PROJECTILE MATERIAL	DIAMETER (mm)	SHIELD MATERIAL	THICKNESS (mm)	SPACING (cm)	BACKUP MATERIAL	THICKNESS (mm)	VELOCITY (km/sec)	TOTAL PENETRATION (mm)	HOLE SIZE (mm)	SPRAY DIAMETER (mm)	SPRAY ANGLE	MV/mv	REMARKS
	2017		1100-0			7075-T6								
E 1	Al	3.18	Al	0.305	5.08	Al	6.35	1.15	1.12	3.33				
2				.635				1.09	1.17	3.61				
3				1.02				1.10	1.17	4.04				
4				1.59				1.10	1.59	4.37				
5				.305				0.72	0.46	3.30				
9							12.7	1.89	1.83	3.74				
10				.635				1.94	1.73	4.65				
11				1.02			6.35	1.87	1.85	4.95				
12				1.59				1.92	2.26	5.82				
13				.305			12.7	2.68	2.64	4.14				
14				.635				2.07	1.83	4.63				
15				1.02			6.35	2.72	2.06	6.05				
16				1.59				2.75	2.16	6.96				
39				.635			2.54	2.56	3.18	4.88				PERFORATED
40							3.18	2.46	3.81	4.86				PERFORATED
41							3.81	2.40	3.58	4.68				
42							4.45	2.52	2.92	4.91				
43				1.02			1.90	2.43	2.92	5.69				PERFORATED
44							2.54	2.65	3.56	5.89				PERFORATED
45							3.18	2.59	2.62	5.87				
46							3.81	2.47	2.57	5.79				
47				1.59			0.81	2.08	2.41	6.02				PERFORATED
48							1.59	2.14	3.20	6.08				PERFORATED
49							2.54	2.12	2.36	6.05				
50							3.18	2.14	1.78	6.05				
51				.635			2.54	1.99	3.18	4.50				PERFORATED
52							3.18	[illegible]	3.20	4.44				

SHOT NO.	PROJECTILE MATERIAL	DIAMETER (mm)	SHIELD MATERIAL	THICKNESS (mm)	SPACING (cm)	BACKUP MATERIAL	THICKNESS (mm)	VELOCITY (km/sec)	TOTAL PENETRATION (mm)	HOLE SIZE (mm)	SPRAY DIAMETER (mm)	SPRAY ANGLE	MV/mv	REMARKS
E-53	2017 Al	3.18	1100-0 Al	0.635	5.08	7075-T6 Al	3.81	1.90	2.44	4.50				
54	〃	〃	〃	〃	〃	〃	4.45	1.90	2.16	—				SABOT HIT